Structure, thermodynamic and transport properties of molten Mg_2SiO_4: Molecular dynamics simulations and model EOS

G. Ben Martin[1,*], Frank J. Spera[1], Dean Nevins[1], Mark S. Ghiorso[2]
[1]Department of Earth Science, University of California-Santa Barbara,
[2]OFM-Research Inc., Seattle
*E-mail: gbenmartin@umail.ucsb.edu

ABSTRACT
Molecular Dynamics simulations have been used to study the structure, equation of state (EOS), self-diffusion and shear viscosity of molten Mg_2SiO_4 for pressure and temperature in the range 2.5-110 GPa and 2100-5060 K, respectively. The transferable pair-potential parameters of Matsui (1998) for the system Na_2O-CaO-MgO-Al_2O-SiO_2 have been used accounting for Coulomb, Born and van der Waals forces. Simulations have been carried out in the NEV ensemble at 63 state points along 12 isochores spanning the density range 2754-4500 kg/m^3. Thermodynamic properties including the isochoric heat capacity, isobaric expansivity, isothermal compressibility, thermal pressure, and the Grüneisen parameter are computed directly from MD results. A density crossover between molten Mg_2SiO_4 and forsterite crystals occurs at ~15 GPa at 2100 K. The Grüneisen parameter (γ) is a function of temperature, increasing with increasing *T* at low density (ρ< 3400 kg/m^3) but decreasing as *T* rises at high density (ρ > 3400 kg/m^3). The integrated form of the Mie-Grüneisen EOS requiring constancy of γ is only approximately valid for liquid Mg_2SiO_4 since γ varies by ~20% over the *T* range 2000-5000 K along an isochore. Radial distribution functions for all atoms around all other atoms were used to generate coordination statistics as a function of *P* and *T*. Oxygen about Si coordination increases from Si(IV) at low pressure to octahedral Si at higher pressure; the abundance of distorted trigonal bipyramidal five-fold polyhedra, Si(V) maximizes at 30 GPa at 3500 K. Interestingly, O about O increases to a maximum of 13 at low *P* before decreasing with increasing pressure to ~ 10. The mean CN of Si around oxygen increases from 1.2 to 1.5 consistent with an increasing abundance of Si_2O_7 dimers as pressure increases. Self-diffusion of Mg, Si and O was calculated at each state point and the results were used to obtain activation energy (67 kJ/mol, 79 kJ/mol and 76 kJ/mol, respectively) and activation volume at zero pressure (7.14×10^5 mol/m^3, 9.1×10^5 mol/m^3, 7.7×10^5 mol/m^3). The fit to an Arrhenian expression with a pressure-dependent activation volume is excellent ($R^2 > 0.98$) for each atom. Shear viscosity of the liquid was calculated at 12 state points using the Green-Kubo formulation. Values give an excellent modified Arrhenian fit for viscosity. Viscosity varies by a factor of ~20 (1.5×10^{-3} Pa s to 0.03 Pa s) at 4000 K as pressure increases from 1 bar to 100 GPa. The modified Arrhenian expression with $E^* = 41$ kJ/mol and a pressure–dependent activation volume $V^* = v_o^* + v_1^* p$ ($v_o^* = 1.46$ cm^3/mol, $v_1^* = -0.005$ cm^{3}mol^{-1} GPa^{-1}) provides an excellent fit to viscosity. The validity of the Stokes-Einstein and Eyring expressions for atom mobility and shear viscosity has been examined in detail. Characteristic lengths for atom mobility are consistent with ionic radii to within a factor of ~ 1.5-2 for all atoms. An equation of state and thermodynamic model for Mg_2SiO_4 liquid is developed by extending a parameterization of the Universal EOS along a reference isotherm with temperature dependent terms that are internally consistent with the fundamental measure functional theory of Rosenfeld and Tarazona (1998). Our model reproduces the *E-P-V-T* relations and the derived thermodynamic properties obtained from the MD simulations to within the reported uncertainty.

Keywords: forsterite liquid, equation of state, molecular dynamics, grüneisen parameter, structure, viscosity, diffusion

INTRODUCTION

An understanding of the equation of state, atomic structure and transport properties of molten silicates in geochemical systems is central to many aspects of planetary dynamics. Quantitative information bearing on the shear viscosity, self-diffusion coefficients, and thermal and ionic conductivities of molten silicates, including the relationship between atomic level structure and macroscopic property variation with pressure (P) and temperature (T), is indispensable in the analysis of geochemical processes. For example, understanding the cooling and crystallization of Earth's early magma ocean requires knowledge of the thermodynamic and transport properties of MgO-rich silicate liquids at P and T in the range 0-135 GPa and 2000-6000 K, respectively. Even higher pressures are important in modeling 'Super-Earth' exoplanets, many of which will probably be discovered in the next decade (Valenci, et. al 2007). The state of the mantle following magma ocean solidification sets the initial conditions for growth and subsequent evolution of the lithosphere, continental and oceanic crust, the hydrosphere and the atmosphere and impacts the start of subduction and the plate tectonic cycle on Earth (e.g., Anderson, 2007). Because silicate liquids are generally more compressible than crystals of the same composition, a density crossover between magma and crystals might be anticipated at high pressure. It is possible therefore that crystalline olivine accumulated in a region of neutral buoyancy in the Earth's primitive magma ocean during and immediately following Earth accretion and Giant Moon-forming impact. Arguments have been presented for the presence today of regions of melt along the Earth's core-mantle boundary (Thorne, et. al 2004). Predictive models for the

properties of multicomponent silicate melts are evidently useful for addressing a variety of primary geochemical problems.

In addition to its importance in geoscience problems, an understanding of the amorphous state (both liquids and glasses), specifically the relationship between structure, the equation of state (EOS) and transport properties, is of intrinsic interest in its own right. Liquid-liquid phase separation in which two liquids of distinct composition coexist are common in multicomponent natural systems (e.g., Roedder 1951; Philpotts 1976). There is now growing interest in the more unusual situation of polyamorphism, a phenomenon whereby a one-component system can exist with at least two liquid or amorphous phases having the same chemical composition but with distinct densities. Phase transitions between liquids occur *without change in composition* but instead with a change in density as temperature or pressure are varied (Tanaka 2000). Experimental evidence for polyamorphism has been found in a number of systems including molten silica, H_2O and binary melts in the system Al_2O_3-Y_2O_3 (Aasland and McMillan 1994; Senker and Rossler 2001; Debenedetti 1996). The existence or lack of polyamorphism can be predicted from critical point analysis of the thermodynamic EOS. Molecular Dynamics simulation has proved to be a useful tool for searching for possible liquid-liquid phase transitions in silicate melts (Saika-Voivod et al. 2000; Skibinsky et al. 2004). Here we extend this search to molten Mg_2SiO_4 by performing a sufficient number of MD simulations to enable accurate derivation of its equation of state needed to assess polyamorphism in molten Mg_2SiO_4. Many additional aspects of the liquid state remain to be explored. Most significant to geochemical systems is the profound reorganization of melt structure upon pressure increase. Atomic-level structural modifications exert a first-

order influence on the melt properties that, in turn, play important geodynamical roles. A better understanding of the liquid state is clearly applicable to many first-order geodynamical issues.

In this study, the structure and properties of liquid Mg_2SiO_4 at elevated P and T are computed by Molecular Dynamics simulation and compared to laboratory results. Additionally, the MD-derived EOS data are used to build comprehensive expressions for the equation of state, internal energy and related thermodynamic properties of liquid Mg_2SiO_4 and to investigate the possibility of a liquid-liquid phase transition. The transferable pair-potential model of Matsui (1998) for the system Na_2O-CaO-MgO-Al_2O_3-SiO_2 is used to study liquid Mg_2SiO_4 at density (ρ), T and P in the range 2754-4500 kg/m^3, 2100–5000 K and 2-110 GPa, respectively. The properties of liquid Mg_2SiO_4 have been computed at 63 state points along 12 isochores utilizing 50 ps duration equilibrium or metastable liquid MD simulations. A first nearest neighbor analysis of Mg, Si and O as a function of density (pressure) along several isotherms is presented. Thermodynamic parameters including the isochoric heat capacity, the Grüneisen parameter, the isothermal compressibility and isobaric expansivity are presented in tabular form at all of the state points studied. Self-diffusivities of Mg, Si and O are used to compute activation energies and volumes and the connection between self-diffusion and short-range melt structure is elucidated. In addition, twelve 'long-duration' MD simulations of 2 nanoseconds (ns) were made to compute the shear viscosity by the Green-Kubo method as a function of temperature and pressure. These long-duration simulations enable a test of the applicability of the Stokes-Einstein and Eyring relations between self-diffusivity of Mg, Si and O and melt shear viscosity and afford a

comparison between the activation energy and volumes for self-diffusion and viscous flow.

MOLECULAR DYNAMICS SIMULATIONS: POTENTIALS AND COMPUTATIONAL DETAILS

A detailed description of the Molecular Dynamics (MD) method with details regarding the implementation and protocol used in this study may be found in Spera et al. (2009). Here we briefly present relevant details pertinent to Mg_2SiO_4 liquid. The potential used in this study is the semi-empirical pair potential of Matsui (1998) for the system Na_2O-CaO-MgO-Al_2O_3-SiO_2. The functional form of the potential includes contributions from long-range Coulombic forces, short-range Born-Mayer exponential repulsion and van der Waals dipolar attractive forces. The potential between two atoms *i*-*j* is:

$$\Phi_{ij}(r_{ij}) = \frac{q_i q_j e^2}{4\pi\varepsilon_o r_{ij}} + A_{ij}\exp(-\frac{r_{ij}}{B_{ij}}) - \frac{C_{ij}}{r_{ij}^6} \qquad (1)$$

where ε_o is the permittivity of free space, r_{ij} is the distance between atom *i* and *j*, q_i is the charge of the i^{th} atom, and A_{ij}, B_{ij} and C_{ij} are parameters that quantify the short-range energetics of atom pair *ij*. Figure 1 shows the potential energy as a function of interatomic distance (*r*) for Mg-O, Si-O and O-O interactions. The potential form is radially-symmetric and pair-wise additive. Fractional charges are used in the MD simulations, with $q_O = -0.945$, $q_{Mg} = 0.945$, and $q_{Si} = 1.89$. The parameters used to define the potential energy interactions are given in Table 1. Details on how the potential was derived may be found in Matsui (1994, 1998).

Molecular Dynamics simulations were performed using 8001 atoms (1143 formula units) in the microcanonical (NEV) ensemble. Each MD run followed the same

protocol: (1) initial positions were configured with atoms in random positions, (2) the system was run at a fixed temperature of 10000 K for 2 picoseconds (ps) to remove excess energy (3) the resulting configuration was run for 2 ps to stabilize following removal of residual net momentum (4) the system was then cooled to the desired temperature using velocity scaling for ~12 ps (5) finally, a 50 ps production simulation was carried out on the equilibrium liquid. Steps (2)-(5) were run using a timestep of 1 femtosecond (fs). All simulations were carried out at fixed volume (density). To verify that thermal equilibrium was achieved for each 50 ps production run, the average simulation temperature was computed for the first and last 10 ps of each 50 ps production run. The two temperature averages were always within the intrinsic temperature fluctuation of the specified simulation (σ_T), in fact usually much closer (3-5 K). Atom trajectories were saved at 10 fs intervals as was temperature (T), pressure (P), kinetic energy (U_K), isochoric heat capacity (C_V) and potential energy (U_P). The fluctuations in temperature (σ_T) and pressure (σ_p) due to the finite size system were calculated at the end of each run. Fluctuation theory informs us that σ_T and σ_p scale as $N^{-1/2}$ where N is the number of atoms used in the simulation (McQuarrie 2000). The $N^{-1/2}$ scaling implies, for example, that σ_T and σ_p are four times smaller in a MD simulation of 8000 atoms compared to one with 500. Using too small an N introduces unacceptable uncertainties in MD state point coordinates (P and T) and directly propagates into uncertainties in thermodynamic and transport properties and into structural states defined by nearest neighbor coordination statistics. The fluctuations for each run are gathered in Table 2 (Electronic Appendix); typically, σ_T is ~ 25 K and σ_p ~ 0.25 GPa. These values represent the intrinsic uncertainty to all state points in this study given the potential parameters of

Table 1. Note that these uncertainties are generally smaller than those of many laboratory experiments at the conditions of elevated T and P explored in this study.

RESULTS

Thermodynamic Properties

The essential results for each equilibrium simulation are presented in Tables 2 and 3 (Electronic Appendix). Figure 2 gives the location in P-T coordinates of sixty-three state points along the 12 isochores studied. The isochores are very slightly non-parallel implying there is a weak density (or pressure) dependence of the slopes of these curves (see the discussion of thermal pressure below). In the appendix we develop an equation of state (EOS) and thermodynamic model from the U-P-ρ state point data. Below, we evaluate some of the important thermodynamic quantities that may be derived from the MD simulation results.

The ρ-P-T results are re-plotted in Figure 3 to demonstrate the density variation with respect to pressure along the seven isotherms studied. These data points are interpolated and extrapolated by the EOS developed in the Appendix as shown. Our results are offset to higher pressures with respect to the empirical potential MD simulations of Lacks et al. (2007) and Belonoshko and Dubrovinsky (1996; not shown). Within the error of the DFT MD results of de Koker et al. (2008), our state points are in agreement at low-P, and systematically displaced to higher pressures at elevated P. All of the MD results shown in Figure 3 are in disagreement with the zero pressure volume of Mg_2SiO_4 liquid inferred from the analysis of the fusion curve, as estimated by Ghiorso (2004).

Thermal pressure. The near-linearity of the P-T coordinates on Figure 2 implies that the thermal pressure, $\left(\frac{\partial p}{\partial T}\right)_V = \frac{\alpha}{\beta} = \alpha K$, where α is the isobaric expansivity, $\alpha \equiv \rho^{-1}\left(\frac{\partial \rho}{\partial T}\right)_p$, β is the isothermal compressibility, $\beta \equiv -\rho^{-1}\left(\frac{\partial \rho}{\partial p}\right)_T$, and K is the bulk modulus, is nearly constant along an isochore. Values of the thermal pressure were computed by centered finite difference methods at interior points and by backward and forward finite difference at the extremes. These values are presented in Table 3 (Electronic Appendix) and illustrated in Figure 4. The thermal pressure varies by about a factor of three from ~ 0.003 GPa/K at low density (2754 kg/m^3) to ~ 0.01 GPa/K at high density (4500 kg/m^3).

Isothermal compressibility and isobaric expansivity. Because the temperatures at which simulations were carried out along each isochore are the same within the temperature fluctuation, σ_T, the isothermal compressibility can be estimated at each state point. Finite difference methods were to compute β (P,T) at each state point from its definition. Values are collected in Table 3 (Electronic Appendix). Values decrease along isochores as T and P increase. Along a low-density isochore (e.g., ρ=2754 kg/m^3), β decreases by a factor ~ 2 as T and P increase (2100→5040 K and 2→11 GPa, respectively) giving an isothermal bulk modulus (K=β^{-1}) of ~40 GPa to ~65 GPa. The value of K at high melt density (T ∈ [3200→5053K], p ∈ [90→110 GPa]) is ~470 GPa, ten times that of the low-P value. For comparison, the isentropic bulk modulus of forsterite crystals at STP is 128.2 GPa (Poirier 2000).

Combining values of the thermal pressure with those of the isothermal compressibility permits computation of the isobaric expansivity at each state point.

Values of α (P,T) are collected in Table 3 (Electronic Appendix). The isobaric expansivity is larger at low T and P and decrease monotonically along isochores in response to increasing P and T. Values of the expansivity vary from 8 x 10^{-5} K^{-1} to 2.1 x 10^{-5} K^{-1} from lowest to highest p-T conditions; a typical representative value for liquid Mg_2SiO_4 is ~ 4.5x10^{-5} K^{-1}. In comparison, for forsterite crystals, α = 2.5x10^{-5} K^{-1} at comparable p-T conditions (Poirier 2000).

Density inversion. Although the density of molten Mg_2SiO_4 is less than that of crystalline forsterite at low pressure, the compressibility of Mg_2SiO_4 liquid, like most liquids, exceeds that of its crystalline counterpart. This implies the possibility of a density inversion at high pressure where the density of forsterite is less than the density of liquid of identical composition. Obviously in such a case, olivine crystals will float in Mg_2SiO_4 liquid. In Figure 5, the density of crystalline forsterite based on the Vinet EOS determined by Ghiorso (2004) and liquid Mg_2SiO_4 from the MD simulations is shown along several isotherms. In figure 5a, at 2100 K, density inversion occurs at ~ 15 GPa equivalent to a depth on Earth of 430 km near the top of the Transition Zone region. At higher temperature, the neutral buoyancy depth increases; in figure 5c, for example, at 3585 K the neutral buoyancy depth is ~ 35 GPa. Shock-wave studies of liquid Mg_2SiO_4 conducted by Mosenfelder (2007) imply a density inversion at ~ 16 GPa, although the temperature of the shocked liquid is ambiguous.

Internal energy. Energies are computed at each time step and the average for each run is given in Table 2 (Electronic Appendix). The kinetic energy of a classical ionic material in the high temperature limit is $U_K = (3/2)\, n\Re T$, where $\Re$ is the universal gas constant and n is the number of atoms in the formula unit (n = 7). The MD-computed

values for U_K are within 1% of the classical limiting value, not surprising considering the temperatures of the simulations.

Isochoric heat capacity and the Grüneisen parameter. The isochoric heat capacity C_V was computed using centered finite differences to estimate the derivative $C_V \equiv \left(\frac{\partial E}{\partial T}\right)_V$. Isochoric molar heat capacity values lie between 177 J/mol K and 225 J/mol K with a mean value of 200 J/mol K over the P-T range of the simulations. This mean value can be compared to the extrapolated value for the isobaric molar heat capacity of forsterite crystals of 206 J/mol K (Poirier 2000). Using the heat capacity in combination with the isothermal compressibility and isobaric expansivity, the Grüneisen parameter (γ) is computed from its definition $\gamma = \frac{\alpha V}{\beta C_V}$; values are given in Table 3 (Electronic Appendix). The validity of the empirical power-law expression relating the Grüneisen parameter to the melt density (e.g., Birch 1952; Anderson 1979; Quareni and Mulargia 1988) can be tested. The empirical relation is $\gamma = \gamma_o (\rho/\rho_o)^q$. Using simulation MF-1 for reference conditions the fit gives q =1.29 and γ_o = 0.86 (R^2 = 0.96). At STP, forsterite crystals have γ_o = 1.18 for comparison (Anderson 2007). Due mainly to the larger compressibility of liquid Mg_2SiO_4 compared to crystals, the reference Grüneisen parameter is somewhat smaller. Our values for the Grüneisen parameter fall within the limits of those measured for molten Mg_2SiO_4 by the shockwave experiments of Mosenfelder et al. (2007). For example, they found γ's ~ 0.4-1.2 at 3000 kg/m^3 and 1.4-2 at 4500 kg/m^3, whereas our results give a range of 0.88-1 and 1.43-1.57 respectively.

Finally, we can test the validity of the Mie-Grüneisen EOS. Recall that the thermal pressure is related to γ by the definition

$$\left(\frac{\partial p}{\partial T}\right)_V = \gamma \frac{C_V}{V} \qquad (2).$$

Integrating at constant volume and assuming for the moment that γ is a constant, the Mie-Grüneisen EOS is obtained in the form

$$P_2 - P_1 = \frac{\gamma}{V} \int_{T_1}^{T_2} C_V \, dT \qquad (3).$$

In order to apply this form of the Mie-Grüneisen EOS the product γρ must be constant along an isochore. In figure 6, this quantity is plotted *versus* pressure. In fact, there is a temperature dependence of γρ such that for ρ < 3400 kg/m^3, γ increases as T increases whereas for ρ > 3400 kg/m^3, the opposite holds. Quantitatively, there is a change of circa 15-20% in the product γρ from 2000- 5000 K. This change indicates that the simple form of the Mie-Grüneisen EOS is not adequate for modeling the high temperature properties of liquid Mg_2SiO_4.

Melt Structure

Short-range coordination statistics. Melt structure and its variation with density (or pressure) and temperature can be investigated by examination of the first nearest neighbor coordination statistics or the Coordination Number (CN) of the i^{th} type of atom around every other type of atom, *j* allowing for *i* = *j*. The CN of atom *i* around atom *j* (atom *j* is the central atom) is determined by first identifying for the pair the value of the radial coordinate *r* of the first minimum following the first maximum of the partial radial distribution function (RDF) $g_{ij}(r)$. The radial distribution function expresses the probability of finding an atom of type *i* in a sphere of radius *r* around an atom of type *j*. Because fluctuations in atom position are an intrinsic part of liquid behavior, at a given state point many atom location 'snapshots' are averaged so that robust CN statistics can

be obtained. In this study approximately 50000 snapshots are used to define the RDF for each CN analysis. The definition of the RDF

$$g_{ij}(r) = \frac{1}{4\pi\rho r^2}\frac{d\langle N_{ij}(r)\rangle}{dr} \qquad (4)$$

is used to determine $N_{ij}(r)$, average number of *i* atoms at a distance between *r* and *r* + *dr* from atom *j*. Once the distance to the first minimum of the RDF is known, the CN is calculated by averaging position 'snapshots' at 0.5 ps intervals. The averaging intervals were spaced by 0.5 ps to ensure uncorrelated time averages. In this way, isothermal plots of the coordination number versus pressure can be used to investigate the melt structure as density (or pressure) changes along an isotherm. Coordination numbers of Si, Mg and O around a central O, and oxygen coordinated around central Si and Mg atoms were determined at each state point and are given in figures 7 and 8 at 3500 K and 5000 K as a function of pressure. CN statistics are presented as percentages of the number fraction.

Oxygen as central atom. By atom number and volume, Mg_2SiO_4 is roughly 57% and 86% oxygen, respectively. It is logical therefore to consider the CN's of Si, Mg and O around central oxygens. In figure 7a the coordination of Si around central oxygen is shown at 3500 K and 5000 K as a function of pressure. At low pressure, ~60% of the oxygen has one nearest Si neighbor whereas about 20% of the O is 'free' oxygen (no closest Si neighbors, CN = 0) and 20% of the oxygen is two-coordinated by Si (CN = 2). The fraction of 'free' oxygen (CN = 0) expectedly decreases with increasing pressure. The fraction of CN = 0 oxygen is high, indicating a relatively 'defect-ridden' melt structure consistent with depolymerization.

As pressure increases the fraction of non-bridging oxygen (CN = 1) and 'free' oxygen (CN = 0) decreases whereas the fraction of oxygen with two nearest Si neighbors

(CN = 2) increases as does the oxygen of CN = 3. The stoichiometry indicates that as pressure increases free oxygen (CN = 0) combines with two non-linked tetrahedra (each with CN = 1) to form a tetrahedral dimer in which one oxygen is shared by two Si. At 80 GPa the fraction of dimmers is about 40%, a result also consistent with depolymerization and one that matches very well results from Sen and Tangeman (2008) who used molecular dynamics simulations of Mg_2SiO_4 liquid at 2273 K and the NMR spectrum of ^{29}Si in Mg_2SiO_4 glass to estimate a dimer (Si_2O_7) fraction of 40%. The number of oxygen with three nearest neighbor Si increases from a negligible amount to about 10% at 97 GPa. The average CN increases from slightly above unity at low pressure to about 1.44 at the highest pressure studied. Comparison of results at 3500 K and 5000 K indicates that temperature exerts a very weak influence on Si around O coordination statistics; pressure is far more important. The coordination of Mg around oxygen is shown in figure 7b at 3500 K and 5000 K. At low pressure the average coordination number CN_{av} of Mg around O is ~ 3; as pressure increases so does the CN_{av} to a value around 3.6. The higher CN's for Mg compared to Si around oxygen reflects the large size of Mg relative to Si. The steepest change in Mg CN occurs in the range 10-30 GPa. Similar to Si coordination around O, the effect of increasing temperature from 3500 K to 5000 K is weak; the pressure dominates over temperature and exerts a first-order effect on short-range order in molten Mg_2SiO_4.

In figure 7c, the CN of oxygen around oxygen is shown. At low pressures, high coordination oxygen polyhedra predominate; CN_{av}, is about 11. There is a small but statistically significant increase in the fraction of CN = 13 and 14 and a correlative

decrease in CN equal to 9, 10, 11, and 12 near 14 GPa at 3500 K and an analogous but more poorly defined feature at 5000 K.

At pressures greater than about 50 GPa, the abundance of highly coordinated oxygen (CN = 12, 13, and 14) drops off whereas the CN = 9 and 10 oxygen increase in concentration at both 3500 K and 5000 K, although the effect is somewhat muted at 5000 K.

Silicon and Magnesium as central atoms. The coordination of oxygen around a central Si gives direct information regarding the local state of polymerization of a melt. Figure 8a shows the CN of oxygen around a central Si atom at 3500 K and 5000 K. At low pressure, more than 75% of the Si is tetrahedrally coordinated with oxygen, the rest mainly in 5-fold coordination, defining distorted trigonal bipyramidal polyhedra. There is a rapid change in coordination as pressure increases. At ~ 20 GPa, the abundances of four-fold and five-fold Si are equal (~ 45%) and 10% of the Si is in octahedral (CN = 6) coordination. The abundance of CN = 5 peaks at ~ 30 GPa; the abundance of CN = 5 and CN = 6 are equal (45%) at 43 GPa. At high pressure the melt is dominated by CN = 6 with very little tetrahedral oxygen and about 15% CN = 5. There is also about 10% of CN = 7. Trends are rather systematic and smooth. These relationships are preserved at 5000 K although distributions are somewhat broader than at 3500 K and the CN = 5 to CN = 6 crossover occurs at higher pressure, around 60 GPa.

Finally, in figure 8b the coordination of oxygen around Mg is shown at 3500 K and at 5000 K. At low pressure, $CN_{av} \approx 5.5$. As pressure increases the average CN increases and equals ≈ 7.5 near 100 GPa. Octahedrally coordinated Mg attains a maximum at about 20 GPa and decreases systematically as pressure increases. The

number of seven coordinated polyhedra maximize at about 50 GPa, whereas Mg with eight nearest oxygen neighbors attains a maximum at circa 100 GPa. Once again, relations at 5000 K are quite similar except that abundance distributions are somewhat broader.

These observations of the P- and T-dependence of the CN's of Si and Mg are broadly consistent with the DFT MD study of de Koker et al. (2008).

Transport Properties

Self-Diffusivity. Self- diffusion coefficients were computed for all runs using accumulated statistics and the Einstein relation

$$D_i = \lim_{t\to\infty} \frac{\left\langle \sum_i^{N_i} [r_i(t) - r_i(0)]^2 \right\rangle}{6N_i t} \qquad (5)$$

where r_i is the position of atom i and N_i is the number of atoms of type i. The term in angled brackets, the mean-squared displacement (MSD), is calculated for each state point simulation from atom trajectories. MSD plots are very linear in time; the Fickian diffusion coefficient is readily calculated from the slope. The very early ballistic part of the MSD (approximately the first 100 fs) is disregarded in the calculation of D.

Self-diffusivities for Mg, Si and O at all state points are listed in Table 2 (Electronic Appendix). Self-diffusivities for all atoms at 2500 K and 4500 K for pressure spanning 0-100 GPa are shown in Figure 9. The computer glass transition is approached from the equilibrium (ergodic) liquid at high pressures along the 2500 K isotherm. Mg remains the most mobile species throughout all P-T space. Oxygen and silicon are the slower diffusers. There is a decrease in all diffusivities with increasing pressure along an isotherm. The slope in these coordinates is directly related to the activation volume, V^*.

The variable slope indicates non-Arrhenian behavior over the temperature range of the simulations.

The MD data are well fit by a modified Arrhenian transport model. The expression is:

$$D = D_o \exp\left(\frac{-(E^* + [v_o^* + v_1^* P]P)}{\Re T}\right) \qquad (6)$$

where $\Re$ is the gas constant, E* is the activation energy for diffusion, and the activation volume V* is a function of pressure only, $V^* = v_o^* + v_1^* p$. v_o^* is the activation volume at zero pressure and v_1^* is the pressure–derivative of the activation volume for diffusion. Values and statistics computed by regression for E^*, D_o and V^* are collected in Table 4. Other parameterizations such as allowing for temperature dependence of V^* do not improve the fit; activation volume depends principally on pressure ($R^2 > 0.98$ for Mg, Si and O). Activation energies are in the range 67-79 kJ/mol with Mg exhibiting the lowest activation barrier. The zero pressure activation volume v_o^* is in the range 1.1-1.4 cm^3/mol and is largest for Mg and smallest for Si; for each GPa of pressure increase the activation volume *decreases* by ~ 0.005 cm^3/mol for Mg and ~0.003 for Si (i.e., $v_1^* = -2.6 \times 10^{-3}$ cm^3/mol GPa). The atom with the largest zero-pressure activation volume (Mg) also possesses the largest pressure-derivative of the activation volume (v_1^*), an activation volume compensation effect.

Shear viscosity. The shear viscosity was calculated at pressure spanning 7-30 GPa and temperatures 3000-4000 K using the Green-Kubo formulation following the procedures of Nevins and Spera (2007). Long simulations, up to 2 nanoseconds (2 ns), were required for acquisition of robust statistics. In the Green-Kubo method, the temporal decay of the five independent stress auto-correlation functions are related to the

dynamical relaxation time and hence the shear viscosity. Viscosity isotherms are shown in Figure 10. The shear viscosity increases with increasing pressure along an isotherm and decreases with increasing temperature along an isobar. At any temperature, the viscosity increases by a factor of ten per 70 GPa increase in pressure. Multiple linear regression was used to determine the activation energy (E_η^*) and activation volume (V_η^*) for viscous flow. The modified Arrhenian expression that correlates the MD values very well is:

$$\eta = \eta_o \exp\left(\frac{(E_\eta^* + [v_{\eta_o}^* + v_{\eta_1}^* p]p)}{\Re T} \right) \qquad (7)$$

which is similar to Eq (6). Note the subscript on the activation energy and volume in Eq (7) used to differentiate the activation quantities for viscous flow and diffusion. In general, the activation energies and volumes for diffusion and viscous flow are independent. The parameters of the fit are given in Table 4. The correlation coefficient $R^2 = 0.998$ indicates the modified Arrhenian form is an excellent model. Interestingly, the activation energy for viscous flow is slightly more than half that for self-diffusion of Mg, Si and O. This observation suggests that cooperative mobility of Mg, Si and O may be important as a viscous flow mechanism. Careful examination of tagged particle dynamics (not attempted in this study) is needed to better understand the differences in the activation energy for diffusion (E^*) *versus* that for viscous flow (E_η^*). In contrast, the activation volume for viscous flow is almost equal to that for self-diffusion falling between the comparable values for O and Mg. The shear viscosity of molten Mg_2SiO_4 at 4000 K increases by a factor of 20 as pressure increases from 1 bar (10^{-4} GPa) to 100 GPa.

Self-diffusion and viscous flow. Because self-diffusivity and shear viscosity are computed independently, the data can be used to test the validity of the Stokes-Einstein (SE) and related Eyring (EY) relations between self-diffusion, shear viscosity and characteristic size of the mobile species.

The Stokes-Einstein relation relates the mobility of an atom (i.e., Mg, Si, or O) to the frictional force exerted on the atom as it diffuses through a continuum medium of viscosity η. The model is often used to estimate self-diffusivity when shear viscosity is known or *vice versa*. In the model, the frictional force exerted on a 'particle' is $f = 6\pi\eta a$ (no slip boundary) or $f = 4\pi\eta a$ (slip boundary), where *a* is the radius of the diffusing particle. For a sphere, *a* is the particle radius. The frictional force is related to the self-diffusion coefficient according to $f = kT/D$ where *k* is the Boltzmann constant. Equating the frictional force expressions gives a relationship between melt viscosity, self-diffusivity and particle size atoms. For a simple Stokes-Einstein fluid, *a* is constant. The expression is

$$a = \frac{kT}{6\pi D\eta} \qquad (8a)$$

for no slip boundary condition and

$$a = \frac{kT}{4\pi D\eta} \qquad (8b)$$

when slip conditions prevail. Implicit in the constancy of *a* in eq (8) is that the P-T dependence of the shear viscosity and the self-diffusivity of oxygen precisely offset one another and that the size of the diffusing 'species' is constant.

In Figure 11, the Stokes-Einstein size parameter *a* is plotted *versus* pressure for Mg, Si and O at 3000 K and 5000 K. If the SE expression is valid, then the data should

define a trend with zero slope and characteristic lengths should approximately equal the ionic radii of Mg, Si or O. In fact, the slopes are near zero with very slight dependence upon pressure, agreeing with the SE expectation. Comparing isotherms at low and high temperatures shows little dependence on temperature. Moreover, the size parameter for each species is correct within a factor of two if we identify the characteristic length as the ionic radius of the appropriate ion. That is, values of the characteristic length *a* for O, Mg, and Si from Figure 11 at 4000 K are ~ 0.8 Å, 1.6 Å, and 1.3 Å, and compare reasonably well to the ionic radii of 0.86 Å, 0.54 Å and 1.26 Å. The only anomaly is in the ordering; one would expect $a_O > a_{Mg} > a_{Si}$ whereas from Figure 11, $a_{Si} > a_O > a_{Mg}$. This anomaly may signify that Si does not diffuse independently of oxygen but instead Si mobility depends cooperatively on oxygen motion.

The Eyring model is similar to the SE model although it is based on a somewhat more detailed atomic level mechanism (e.g., Eyring 1982). Applied to molten Mg_2SiO_4 the relationship between self-diffusivity and viscosity is:

$$\frac{kT}{(V/nN_A)^{1/3} D\eta} = \xi \qquad (9)$$

where n is the number of atoms per formula unit (n = 7), V(P,T) is the molar volume at the state point at which the atom diffusivity and shear viscosity are evaluated and N_A is Avogadro's number. In a simple fluid, such as liquid argon, for example, ξ represents the number of nearest neighbors surrounding a central diffusing atom that are pushed aside during the atom hopping event. Typically, ξ takes on values in the range 6-12 in simple fluids. For Mg_2SiO_4 liquid, ξ presumably represents some suitable average CN. If we consider molten Mg_2SiO_4 as essentially an oxygen superlattice glued together by high field strength Si, values of ξ within the range of the CN_{av} of O around central Si (~5-6,

Figure 7) and the CN_{av} of O around O (~ 12, Figure 8), one might expect a value of ξ around 10. In this admittedly simplistic view, melt is pictured as an oxygen superlattice that governs the kinetics of flow and atom mobility. This notion is not exactly correct, of course, but seems like a reasonable first-approximation to a more complicated picture. In Figure 12, computed values of ξ are shown for several isotherms as a function of pressure. The values of ξ for O and Si are around 8 which is broadly consistent with the coordination statistics of Figures 7 and 8. In light of the crudity of the Stokes-Einstein and Eyring models applied to structured molten silicates, the broad agreement between MD results and these elementary mechanistic theories is surprisingly good. Whether this is coincidental can only be better appreciated by applying the theory to other compositions such as molten $MgSiO_3$ and molten $CaAl_2Si_2O_8$ (Spera et al 2009; Nevins and Spera 2009).

CONCLUSIONS

We carried out pair-potential molecular dynamics simulations of liquid Mg_2SiO_4 along 12 isochores at 63 state (P,T) points at T from 2100-5000 K and P from 2-110 GPa using the transferable potential model of Matsui (1998). The MD results were used to compute the thermal pressure, isobaric expansivity, isothermal compressibility, isochoric heat capacity, Grüneisen parameter, and the internal energy of molten Mg_2SiO_4 over a range of conditions corresponding to the Earth's mantle. Values are compiled in tabular form (Electronic Appendix) at all MD state points. An equation of state and a self-consistent thermodynamic model is developed from these data. The model is based upon the Universal EOS of Vinet et al. (1986; 1987; 1989) and the potential energy scaling relation of Rosenfeld and Tarazona (1998). A crystal-liquid density cross-over near 15

GPa at 2100 K is predicted. The ratio of the Grüneisen parameter to the molar volume is not constant as demanded by the simple integrated form of the Mie-Grüneisen EOS but instead varies by ~ 20% over the temperature range 2000-5000 K.

Profound changes in melt structure at the atomic level take place in response to increasing pressure; temperature effects, although present, are much less important. For example, along the 3500 K isotherm, the fraction of Si (IV), Si (V), and Si (VI) first-coordination polyhedra changes from 78%, 20%, and 2% at 5 GPa to 1%, 18%, and 80%, respectively at 95 GPa. The abundance of 5-fold oxygen present attains a maximum at ~ 30 GPa at 3500 K. Oxygen packing around central Mg follows similar trends although the mean coordination number is higher with Mg (IV) and Mg (VI) decaying monotonically with increasing pressure. Mg (VI) attains a maximum at 20 GPa and Mg (VII) and Mg (VIII) increase monotonically with increasing pressure. The mean CN of O around Mg of ~ 5.5 at low P increases to ~ 7.5 at 90 GPa. The packing of Si around central oxygen also shows systematic changes with increasing pressure. At P ~ 5 GPa, 60% of the Si has one nearest O neighbor whereas 20% of the Si has either two (Si_2O_7 dimer) or no oxygen as a nearest neighbor. Polymerization occurs as pressure increases as two SiO_4 tetrahedra condense to form a dimer and produce a free oxygen. Hence at 5 GPa, 80% of the oxygen is non-bridging oxygen (NBO) and the fraction of bridging oxygen (BO) is ~ 20%. In contrast, at 90 GPa about equal amounts of BO and NBO coexist. The mean CN of Mg around central oxygen shows relatively little variation except for a modest increase from ~ 3 to ~ 3.6 in the pressure range 5-100 GPa at 3500 K. In contrast the coordination of oxygen around other oxygen reveals two interesting features. The mean CN of O around O at low P (5GPa) is ~ 11.5 with O (XI, XII and

XIII) dominating. At P corresponding to the crystalline polymorphic inversion of olivine to β-spinel structure, the abundance of O (IX), O (X), O (XI), and O (XII) all decrease abruptly whereas O (XIII) and O (IVX) increase in abundance. At about 40 GPa O (IX) and O (X) increase such that the mean CN at 100 GPa is ~10, *lower* than the mean oxygen around oxygen CN at 5 GPa.

Self-diffusivities for Si, Mg and O are fit to a modified Arrhenian expression and exhibit monotonic decrease along an isotherm. Activation energies are in the range 67-79 kJ/mol with Mg exhibiting the lowest activation barrier. The zero pressure activation volume v_o^* is in the range 1.1-1.4 cm^3/mol and is largest for Mg and smallest for Si consistent with ionic radii. The shear viscosity was computed using the Green-Kubo formulation and MD values for the temporal decay of the off-diagonal components of the stress tensor. The shear viscosity follows the modified Arrhenian expression with an activation energy for viscous flow of 41 kJ/mol and a zero-pressure activation volume of 1.5 cm^3/mol, essentially identical to the activation volume for diffusion. The validity of the Stokes-Einstein and Eyring models for relating self-diffusion to shear viscosity have been tested and show reasonable congruity. Data from the MD simulations are used in part 2 to develop a comprehensive EOS for molten Mg_2SiO_4.

Acknowledgements

Material support for this investigation was provided by the National Science Foundation (EAR- 0609680 to MSG). This is OFM Research publication #10.

Captions

Figure 1. Interatomic potentials for Mg-O, Si-O, and O-O pair interactions. The form of the potential is given by eq (1) in text; numerical parameters are given in Table 1 are derived from Matsui (1998).

Figure 2. Location of state points in p-T space investigated by MD simulation in this study. State point uncertainties are identical to T and p fluctuations of $\sigma_T \approx 25$ K and $\sigma_p \approx 0.25$ GPa, respectively. The fusion curve of forsterite is from Ghiorso (2004). Most of the simulations are in the equilibrium liquid field although a few correspond to metastable liquid.

Figure 3. Density estimates for Mg_2SiO_4 liquid. State points computed in this paper are plotted as solid circles. The thin solid curves interpolate and extrapolate these states points using the EOS developed in the Appendix. The results of this paper are compared to the empirical potential MD calculations of Lacks et al. (2007; heavy solid curve) and the DFT MD estimates along three isotherms reported by de Koker et al. (2008). The large striped symbol indicates a zero pressure estimate of the molar volume of Mg_2SiO_4 liquid calculated from the initial slope of the forsterite fusion curve (Ghiorso, 2004).

Figure 4. Thermal pressure coefficient (α/β) plotted versus pressure. MD simulation data are shown with estimated uncertainties. Curves are calculated from the model developed in the appendix. Isotherms are chosen as average temperatures of the simulations.

Figure 5. Density inversion, where the crystalline Mg_2SiO_4 becomes less dense than the liquid phase, shown for different temperatures.

Figure 6. The product of the thermodynamic Gruneisen parameter and liquid density ($\gamma\rho$) plotted *versus* pressure. The non-zero slopes of the MD data arrayed along each isochore show that the simple integrated form of the Mie-Gruneisen EOS requiring constantcy of $\gamma\rho$ is only approximately applicable. MD simulation data are shown with estimated uncertainties. Curves are calculated from the model developed in the appendix. Isotherms are chosen as average temperatures of the simulations.

Figure 7. (a) Si around O coordination statistics along 3583 K and 5043 K isotherms. (b) Mg around O coordination statistics along 3583 K and 5043 K isotherms. (c) O around O coordination statistics along 3583 K and 5043 K isotherms. The solid thatched line represents the average coordination state (CN_{av}) based on the number fractions.

Figure 8. (a) O around Si coordination statistics along 3583 K and 5043 K isotherms. (b) O around Mg coordination statistics along 3583 K and 5043 K isotherms. The solid thatched line represents the average coordination number, CN_{av}.

Figure 9. Self-Diffusivity for O, Mg and Si at 3583 K *versus* pressure. Points represent values derived from MD simulations and curves are based on fit using eq (6) and

parameters from Table 4. The non-linear slope implies a small pressure-dependence of the activation volume for diffusion for all atoms.

Figure 10. Viscosity computed by Green-Kubo method *versus* pressure at 3000-4000 K. Points are from MD simulations; curves represent Arrhenian fits based on eq (7) and Table 4.

Figure 11. Stokes-Einstein plot based on eq (7b) for O, Si and Mg at 3000 K and 5000 K *versus* pressure. The ordinate is the length scale 'c' equivalent to the effective hydrodynamic radius of the diffusing particle. 'c' is approximately constant, consistent with the SE relation. For oxygen, the characteristic length 'c' closely approximates the ionic radius of oxygen.

Figure 12. Parameter ξ, related to the number of neighboring atoms the diffusing entity must push aside to allow flow *versus* pressure based on the Eyring relationship, eq (9). The lack of significant pressure-dependence of ξ is consistent with the expectation from the Eyring model. Values of ξ around 6-10 are expected based on coordination statistics from the MD simulations.

Figure 13. Rosenfeld-Tarazona analysis of potential energy-temperature relations. (A) Comparsion of MD data to parameterizations of the form $U = a + bT^{3/5}$ (Rosenfeld and Tarazona, 1998) for results along 12 isochores. See Table 5. (B) Residuals in U corresponding to the Rosenfeld-Tarazona model expressions when compared to MD simulation results. The uncertainty brackets correspond to those of the MD simulations; model residuals are well within the 1σ brackets.

Figure 14. Polynomial representation of the volume dependence of the Rosenfeld-Tarazona model slopes and intercepts. Uncertainties shown are the statistical uncertainties of the linear fits along each isochore (Table 5). Polynomial coefficients are provided in Table 6. (A) $a(V)$ (B) $b(V)$.

Figure 15. Model EOS recovery of the MD simulaton data. Pressure uncertainty as reported in Table 3. An average simulation temperature is used to calculate each model isotherm: 2112 K, 2580 K, 3082 K, 3583 K (T_0), 4068 K, 4553 K, and 5042 K.

Equation Chapter 1 Section 1

Appendix: Thermodynamic relations and Equation of State

Rosenfeld and Tarazona (1998) derive an expression from a fundamental-measure energy functional for hard spheres and thermodynamic perturbation theory for the functional dependence of the potential energy (U) on volume (V) and temperature (T) in a dense classical liquid:

$$U(V,T) = a(V) + b(V)T^{3/5} \tag{10}$$

This expression beautifully represents the potential energy-temperature relations along a given isochore obtained from our MD simulations of liquid Mg_2SiO_4 (Fig. 13, Table 5).

The *a(V)* and *b(V)* functions may be parameterized using simple polynomials of volume (Fig. 14, Table 6, e.g. Saika-Voivod et al., 2000).

Given the representation of U embodied in Eq. (10), the internal energy, E, is obtained by addition of the kinetic energy, $\frac{3n}{2}RT$, where n in this case is seven, the number of atoms in the formula unit of Mg_2SiO_4 liquid:

$$E(V,T) = a(V) + b(V)T^{3/5} + \frac{3n}{2}RT \tag{11}$$

From Eq. (11) the isochoric heat capacity is readily obtained by differentiation with respect to T at constant V

$$C_V = \frac{3}{5}\frac{b(V)}{T^{2/5}} + \frac{3n}{2}R \tag{12}$$

It should be appreciated that since values of the function $b(V)$ are positive (e.g. Fig 14b), the heat capacity of a Rosenfeld-Tarazona fluid will decrease with increasing temperature asymptotically to the value $3nR/2$.

An internally consistent equation of state (EOS) may be constructed from Eq. (11) by first finding an expression for the Helmholtz free energy (A), which is formally defined as

$$A(V,T) = E(V,T) - TS(V,T) \tag{13}$$

The temperature- and volume-dependence of the entropy (S) may be obtained from Eq. (11) and the thermodynamic identity $dE = TdS - PdV$. From this identity it follows that

$$\left(\frac{\partial E}{\partial V}\right)_T = T\left(\frac{\partial S}{\partial V}\right)_T - P$$

and

$$\left(\frac{\partial E}{\partial T}\right)_V = T\left(\frac{\partial S}{\partial T}\right)_V$$

which together permit the entropy to be evaluated as

$$S(V,T) = S(V_0,T_0) + \frac{1}{T_0}\int_{V_0}^{V}\left[\left(\frac{\partial E}{\partial V}\right)_T\Big|_{T_0} + P(V,T_0)\right]dV + \int_{T_0}^{T}\frac{1}{T}\left(\frac{\partial E}{\partial T}\right)_V dT \tag{14}$$

Substitution of Eq. (11) into Eq. (14) gives a model expression

$$\begin{aligned} S(V,T) = {} & S(V_0,T_0) \\ & + \frac{1}{T_0}\left[a(V) + T_0^{3/5}b(V) - a(V_0) - T_0^{3/5}a(V_0) + \int_{V_0}^{V}P(T_0,V)dV\right] \\ & - \frac{3}{2}\left(\frac{1}{T^{2/5}} - \frac{1}{T_0^{2/5}}\right)b(V) + \frac{3n}{2}R\ln\left(\frac{T}{T_0}\right) \end{aligned} \tag{15}$$

Note that the entropy is defined *relative to that at a reference volume* (V_0) *and temperature* (T_0) – that is, with respect to an unspecified constant - and that the model expression requires adoption of an EOS along the reference isotherm [$P(T_0, V)$]. The selection of this EOS is arbitrary.

Substitution of Eqs. (11) and (15) into Eq. (13) gives a model expression for the Helmholtz free energy compatible with Eq. (10)

$$\begin{aligned} A(V,T) = {} & a(V) + T^{3/5} b(V) + \frac{3n}{2} RT - TS(V_0, T_0) \\ & - \frac{T}{T_0}\left[a(V) + T_0^{3/5} b(V) - a(V_0) - T_0^{3/5} a(V_0) + \int_{V_0}^{V} P(T_0, V) dV \right] \\ & + T \frac{3}{2}\left(\frac{1}{T^{2/5}} - \frac{1}{T_0^{2/5}} \right) b(V) - \frac{3n}{2} RT \ln\left(\frac{T}{T_0} \right) \end{aligned} \tag{16}$$

An EOS is obtained from Eq. (16) by differentiation, i.e., $P = -\left(\frac{\partial A}{\partial V} \right)_T$:

$$P = \left(\frac{T}{T_0} - 1 \right) \frac{da(V)}{dV} + \frac{5}{2} T^{3/5} \left[\left(\frac{T}{T_0} \right)^{2/5} - 1 \right] \frac{db(V)}{dV} + \frac{T}{T_0} P(T_0, V) \tag{17}$$

This result demonstrates that a Rosenfeld-Tarazona compatible EOS – $P(V,T)$ – can be built from any isothermal EOS of choice, and that the temperature dependence of the pressure arises through the parameterization of the potential energy of the fluid. In this paper we adopt for $P(T_0, V)$ the Universal EOS of Vinet at al. (1986; 1987; 1989)

$$P(T_0, V) = \frac{3K_v (1 - x) e^{\eta(1-x)}}{x^2} \tag{18}$$

where $\eta = \frac{3}{2}\left(K_v' - 1 \right)$ and $x = \left(\frac{V}{V_v} \right)^{1/3}$. In Eq. (18), K_v, K_v' and V_v are constants (fit parameters of the EOS), whose values correspond to the bulk modules, its pressure

derivative, and the zero pressure volume, respectively, all at the temperature T_0. A fit to the nominal ~3500 K MD data for Mg_2SiO_4 liquid is presented in Table 7. The model EOS is presented and compared to the MD simulation data in Fig 15.

In the low temperature limit, the Helmholtz energy [Eq. (16)] reduces to $A(V,T) \approx a(V)$, and by inspection of Fig. 14a it is clear that in the case of our model calculations for Mg_2SiO_4 liquid there is a range of volume over which the liquid is thermodynamically unstable with respect to unmixing at sufficiently low-*T*; this region corresponds to the portion of the curve that is concave down, and in this case the coexisting liquids differ in structure but are identical in composition. The loci of (*V*,*T*)-points corresponding to zero-curvature of *A* is known as the spinoidal and is given by the thermodynanic condition of phase instability (Prigogine and Defay, 1954): $\left(\partial P/\partial V\right)_T = 0$, which from Eq. (17) is

$$\left(\frac{\partial P}{\partial V}\right)_T = 0 = \left(\frac{T}{T_0} - 1\right)\frac{d^2a(V)}{dV^2} + \frac{5}{2}T^{3/5}\left[\left(\frac{T}{T_0}\right)^{2/5} - 1\right]\frac{d^2b(V)}{dV^2} + \frac{T}{T_0}\frac{dP(T_0,V)}{dV} \qquad (19)$$

for our thermodynamic model. The highest temerature that satisfies Eq. (19) is the *critical point* (the temperature of the onset of unmixing). We find this *T* to be below 100 K, a condition corresponding to the deeply supercooled region.

A compete set of thermodynamic functions can be developed from Eqs. (16) and (17) and the numerical evaluation of these functions requires no further paramterization of the MD data.

The Gibbs free energy ($G = A + PV$) is

$$
\begin{aligned}
G(V,T) = {} & a(V) + T^{3/5} b(V) + \frac{3n}{2} RT - TS(V_0,T_0) \\
& - \frac{T}{T_0}\left[a(V) + T_0^{3/5} b(V) - a(V_0) - T_0^{3/5} a(V_0) + \int_{V_0}^{V} P(T_0,V)\,dV \right] \\
& + T\,\frac{3}{2}\left(\frac{1}{T^{2/5}} - \frac{1}{T_0^{2/5}} \right) b(V) - \frac{3n}{2} RT \ln\left(\frac{T}{T_0} \right) \\
& + \left(\frac{T}{T_0} - 1 \right) V \frac{da(V)}{dV} + \frac{5}{2} T^{3/5} \left[\left(\frac{T}{T_0} \right)^{2/5} - 1 \right] V \frac{db(V)}{dV} + \frac{T}{T_0} V P(T_0,V)
\end{aligned}
\tag{20}
$$

The coefficient of "thermal pressure," $\left(\frac{\partial P}{\partial T} \right)_V$, is given as

$$
\left(\frac{\partial P}{\partial T} \right)_V = \frac{1}{T_0} \frac{da(V)}{dV} + \frac{3}{2} T^{-2/5} \left[\frac{5}{3} \left(\frac{T}{T_0} \right)^{2/5} - 1 \right] \frac{db(V)}{dV} + \frac{P(T_0,V)}{T_0} \tag{21}
$$

The bulk modulus, $K = -V\left(\frac{\partial P}{\partial V} \right)_T$, is found to be

$$
K = -\left(\frac{T}{T_0} - 1 \right) V \frac{d^2 a(V)}{dV^2} - \frac{5}{2} T^{3/5} \left[\left(\frac{T}{T_0} \right)^{2/5} - 1 \right] V \frac{d^2 b(V)}{dV^2} - \frac{T}{T_0} V \frac{dP(T_0,V)}{dV} \tag{22}
$$

and, since $\alpha K = \left(\frac{\partial P}{\partial T} \right)_V = -\left(\frac{\partial V}{\partial T} \right)_P \left(\frac{\partial P}{\partial V} \right)_T$, the isothermal coefficient of expansion (α)

may be written

$$
\alpha = -\frac{\frac{1}{T_0} \frac{da(V)}{dV} + \frac{3}{2} T^{-2/5} \left[\frac{5}{3} \left(\frac{T}{T_0} \right)^{2/5} - 1 \right] \frac{db(V)}{dV} + \frac{P(T_0,V)}{T_0}}{V \left\{ \left(\frac{T}{T_0} - 1 \right) \frac{d^2 a(V)}{dV^2} + \frac{5}{2} T^{3/5} \left[\left(\frac{T}{T_0} \right)^{2/5} - 1 \right] \frac{d^2 b(V)}{dV^2} + \frac{T}{T_0} \frac{dP(T_0,V)}{dV} \right\}} \tag{23}
$$

Finally, our model expression for the Grüneisen parameter, $\gamma = \frac{\alpha K V}{C_V}$, is given by

88
$$\gamma = \frac{\frac{V}{T_0}\frac{da(V)}{dV} + \frac{3}{2}VT^{-2/5}\left[\frac{5}{3}\left(\frac{T}{T_0}\right)^{2/5} - 1\right]\frac{db(V)}{dV} + \frac{VP(T_0,V)}{T_0}}{\frac{3}{5}\frac{b(V)}{T^{2/5}} + \frac{3n}{2}R} \qquad (24)$$

References

Aasland, S. and Macmillan, P.F. (1994) Density-driven liquid-liquid phase separation in the system Al_2O_3-Y_2O_3, Nature, 369, 633-636.

Agee, C. (1998) Crystial-liquid density inversions in terrestrial and lunar magmas, Physics of the Earth and Planetary Interiors, 107, 63-74.

Anderson, D. (2007) New theory of the Earth, 384 p. Cambridge University Press, New York.

Anderson, O.L. (1979) Evidence supporting the approximation $\gamma\rho$=const for the Grüneisen parameter of the Earth's lower mantle, Journal of Geophysical Research, 84, 3537-3542.

Belonoshko, A.B. and Dubrovinsky, L.S. (1996) Molecular and lattice dynamics study of the MgO-SiO_2 system using a transferable interatomic potential, Geochimica et Cosmochimica Acta, 60, 1645-1656.

Birch, F. (1952) Elasticity and constitution of the Earth's interior, Journal of Geophysical Research, 57, 227-286.

Debenedetti, Pablo (1996) Metastable Liquids: Concepts and Principles, Princeton University Press.

Eyring, H. (1982) Statistical Mechanics and Dynamics, ed. 2, 785 p. Wiley, New York.

Ghiorso, M. S. (2004) An equation of state for silicate melts. III. Analysis of stoichiometric liquids at elevated pressure: shock compression data, molecular dynamics simulations and mineral fusion curves, American Journal of Science, 304, 752-810.

de Koker, N.P., Stixrude, L., and Karki, B.B. (2008) Thermodynamics, structure, dynamics, and freezing of Mg_2SiO_4 liquid at high pressure, Geochimica et Cosmochimica Acta, 72, 1427-1441.

Lacks, D.J., Rear, D.B., and van Orman, J.A. (2007) Molecular dynamics investigation of viscosity, chemical diffusivities and partial molar volumes of liquids along the MgO-SiO_2 join as functions of pressure, Geochimica et Cosmochimica Acta, 71, 1312-1323.

Nevins, D. and Spera F.J. (2007) Accurate computation of shear viscosity from equilibrium molecular dynamics simulations, Molecular Simulation, 33:15, 1261-1266.

Nevins, D. and Spera F.J. (2009) Viscosity of liquid $MgSiO_3$ to the Core-mantle boundary, Geophysical Research Letters (submitted 8/08)

Matsui, M. (1998) Computational modeling of crystals and liquids in the system Na2O-CaO-MgO-Al2O3-SiO2. In M.H. Manghnani and T. Yagi, Eds., Properties of Earth and Planetary Materials at High Pressure and Temperature, 145-148. Geophysical Monograph Series, AGU, Washington, D.C.

McQuarrie, D.A. (2000) Statistical Mechanics, University Science Books.

Mosenfelder, J.L., Asimow, P.D., and Ahrens, T.J. (2007) Thermodynamic properties of Mg_2SiO_4 liquid at ultra-high pressures from shock experiments to 200 GPa on forsterite and wadsleyite,

Ohtani, E., Suzuki, A., and Kato, T. (1998) Flotation of olivine and diamond in mantle melt at high pressure: Implications for fractionation in the deep mantle and ultra deep origin of diamond. In M.H. Manghnani and T. Yagi, Eds., Properties of Earth and Planetary Materials at High Pressure and Temperature, 227-239. Geophysical Monograph Series, AGU, Washington, D.C.

Philpotts, A.R. (1976) Silicate liquid immiscibility: its probable exponent and petrogenetic significance, American Journal Science, 276, 1147-1177.

Poirier, J.P. (2000) Introduction to the Physics of the Earth's Interior, ed. 2, 312 p., Cambridge University Press, Cambridge.

Prigogine, I. and Defay, R. (1954) Chemical Thermodynamics, 543 p. Longmans, Green and Co., New York.

Quareni, F. and Mulargia, F. (1998) The validity of the common approximate expressions for the Grüneisen parameter, Geophysical Journal International, 93, 505-519.

Rosenfeld, Y. and Tarazona, P. (1998) Density functional theory and the asymptotic high density expansion of the free energy of classical solids and fluids, Molecular Physics, 95, 141-150.

Roedder, E. (1951) Low temperature liquid immiscibility in the system K_2O-FeO-Al_2O_3-SiO_2, American Mineralologists, 36, 282-282.

Saika-Voivod, I., Soiortino, F., and Pool, P.H. (2000) Computer simulations of liquid silica: Equation of state and liquid-liquid phase transition, Physical Review E, 63, 011202.

Sen, S. and Tangeman, J. (2008) Evidence for anomalously large degree of polymerization in Mg2SiO4 glass and melt, American Minerologist, 93, 946-949.

Senker, J. and Rossler, E. (2001) Triphenyl phosphate: a candidate for liquid polyamorphism, Chemical Geology, 174, 143-156.

Skibinsky, A., Buldyrev, S.V., Franzese, G., Malescio, G., and Stanley, H.E. (2004) Liquid-liquid phase transitions for soft-core attractive potentials, Physical Review E, 69, 061206.

Spera, F., Nevins, D., Cutler, I., and Ghiorso, M. (2009) Structure, thermodynamic and transport properties of $CaAl_2SiO_8$Liquid: Part I Molecular Dynamics simulations, American Mineralogist (submitted 9/08).

Stolper, E., Walker, D., Hager, B.H., and Hays, J.F. (1981) Melt segregation from partially molten source regions: The importance of melt density and source region size, Journal of Geophysical Research, 86, 6261-6271.

Suzuki, A. and Ohtani, E. (2003) Density of peridotite melts at high pressure, Physics and Chemistry of Minerals, 30, 449-456.

Tanaka, H. (2000) General view of a liquid-liquid phase transition, Physical Review E, 62, 6968-6976.

Thorne, M.S., Garnero, E.J., and Grand, S.P. (2004) Geographic correlation between hot spots and deep mantle lateral shear-wave velocity gradients, Physics of the Earth and Planetary Interiors, 146, 47-63.

Valenci, D., Sasselov, D.D., and O'Connel, R.J. (2007) Radius and structure models for the first super-earth planet, Astrophysical Journal, 656, 545-551.

Vinet, P., Ferrante J., Smith J.R., and Rose J. H. (1986) A universal equation of state forsolids, Journal of Physics C: Solid State Physics, v. 19, p. L467-L473.

Vinet, P., Rose J. H., Ferrante J., and Smith J.R. (1989) Universal features of the equation of state of solids, Journal of Physics: Condensed Matter, v. 1, p. 1941-1963.

Vinet, P., Smith J. R., Ferrante J., and Rose J.H. (1987) Temperature effects on the universal equation of state of solids, Physical Review B, v. 35, p. 1945-1953.

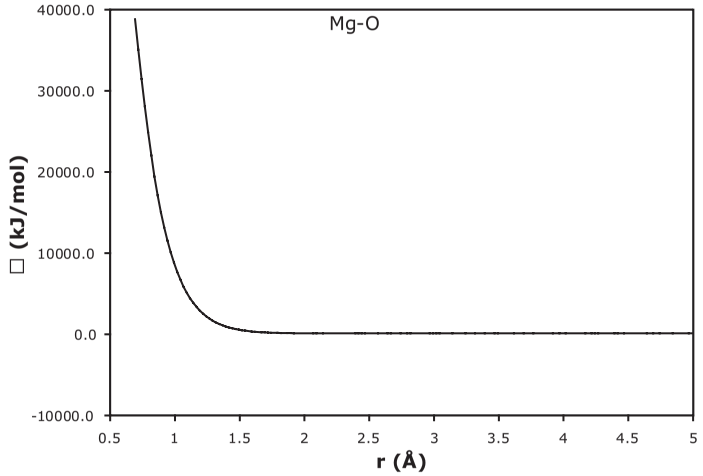
Mg-O
40000.0
30000.0
20000.0
10000.0
0.0
-10000.0
□ (kJ/mol)
0.5
1
1.5
2
2.5
3
3.5
4
4.5
5
r (Å)

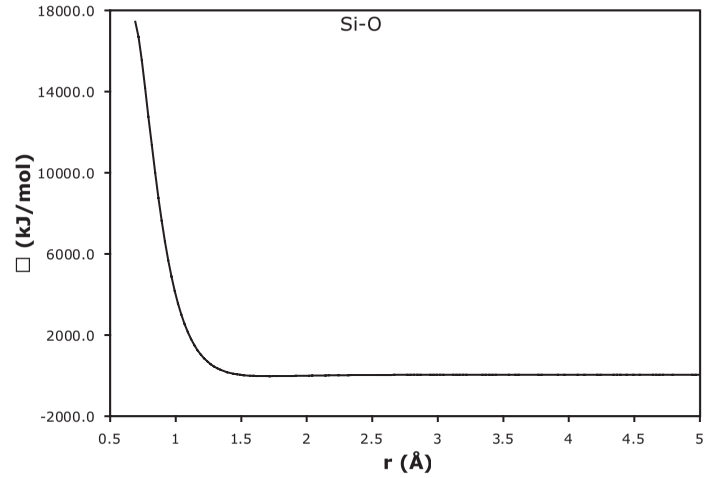
Si-O
18000.0
14000.0
10000.0
6000.0
2000.0
-2000.0
□ (kJ/mol)
0.5
1
1.5
2
2.5
3
3.5
4
4.5
5
r (Å)

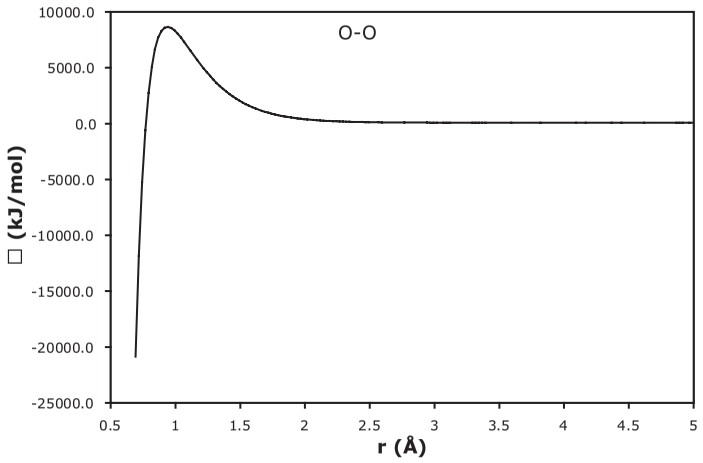
O-O
10000.0
5000.0
0.0
-5000.0
-10000.0
-15000.0
-20000.0
-25000.0
□ (kJ/mol)
0.5
1
1.5
2
2.5
3
3.5
4
4.5
5
r (Å)

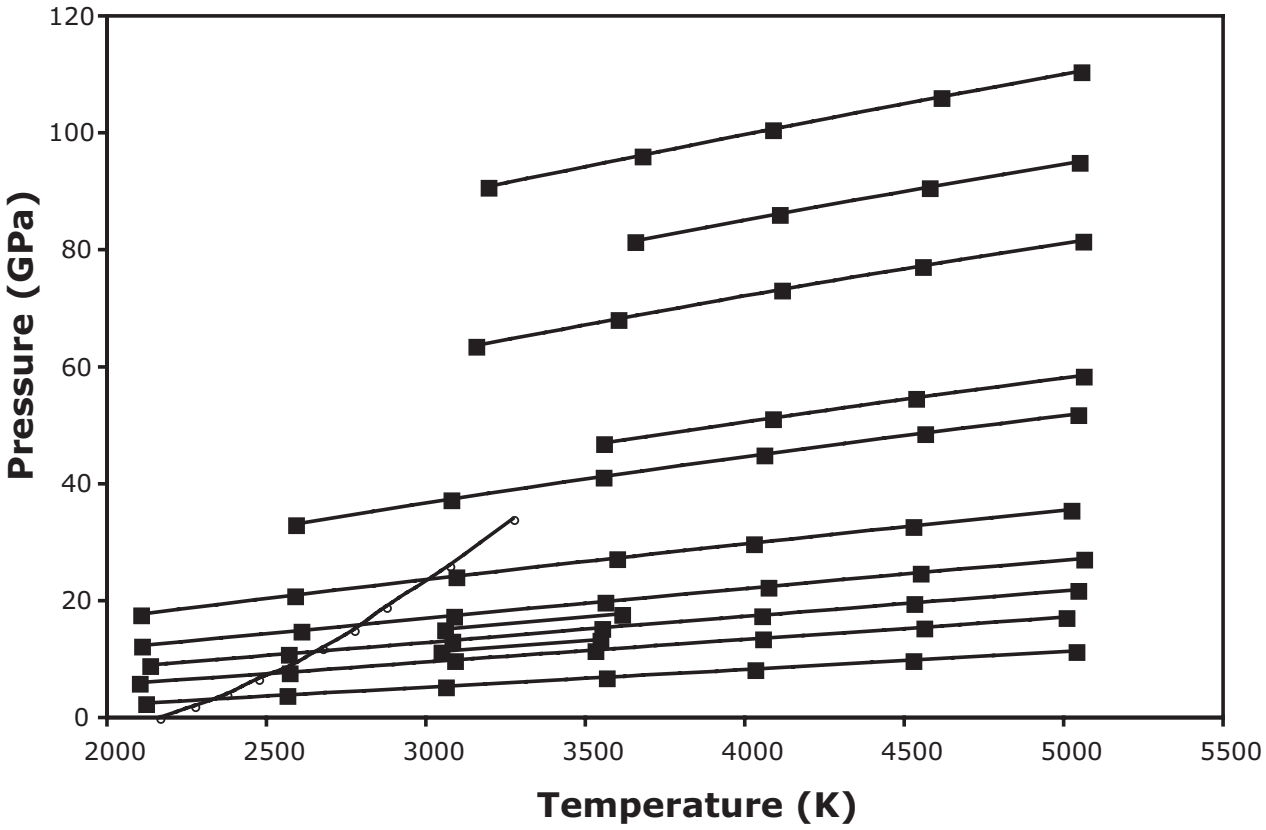
Pressure (GPa)
120
100
80
60
40
20
0
2000
2500
3000
3500
4000
4500
5000
5500
Temperature (K)

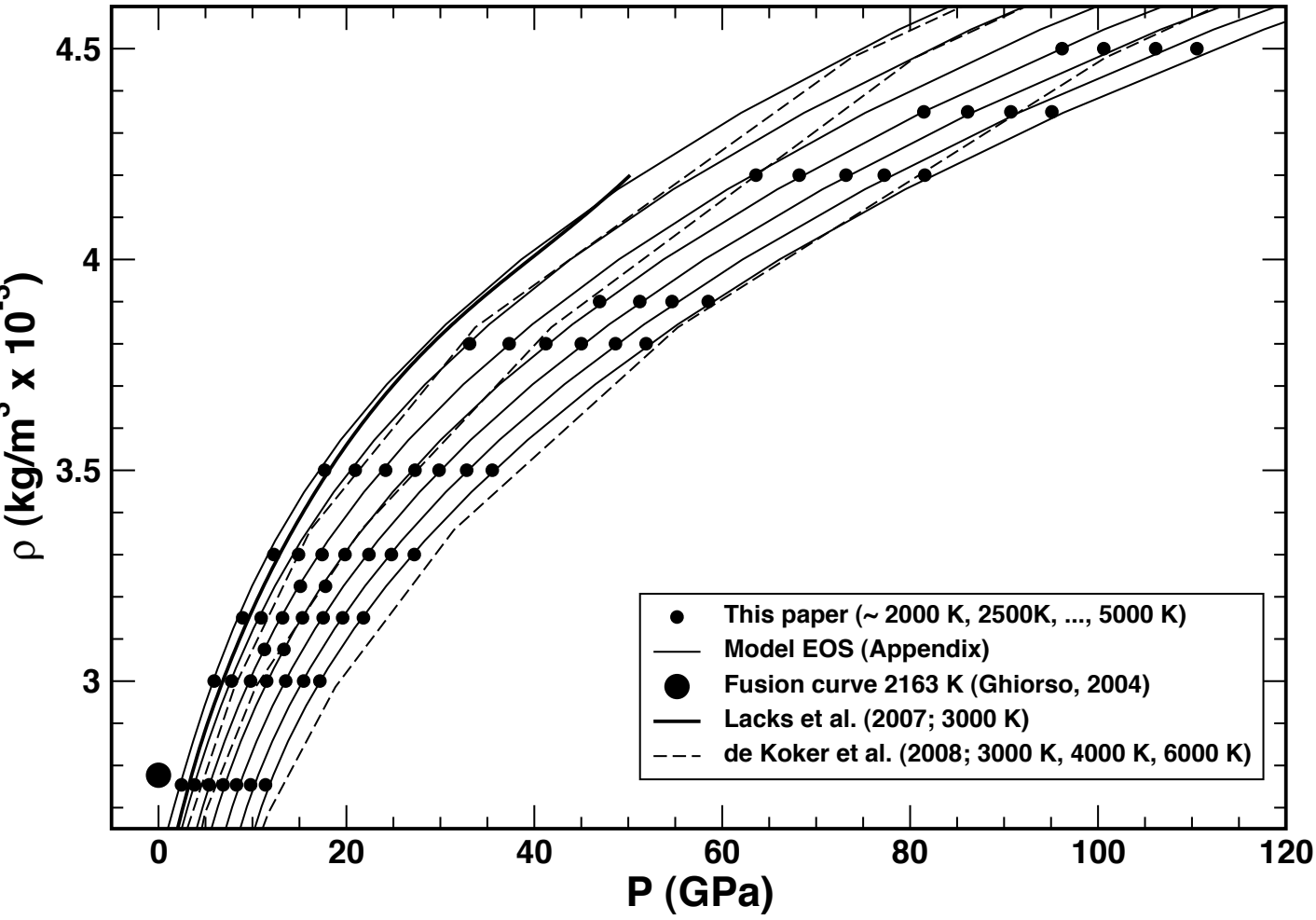
4.5
4
3.5
3
ρ (kg/m3 x 10-3)
0
20
40
60
80
100
120
P (GPa)
This paper (~ 2000 K, 2500K, ..., 5000 K)
Model EOS (Appendix)
Fusion curve 2163 K (Ghiorso, 2004)
Lacks et al. (2007; 3000 K)
de Koker et al. (2008; 3000 K, 4000 K, 6000 K)

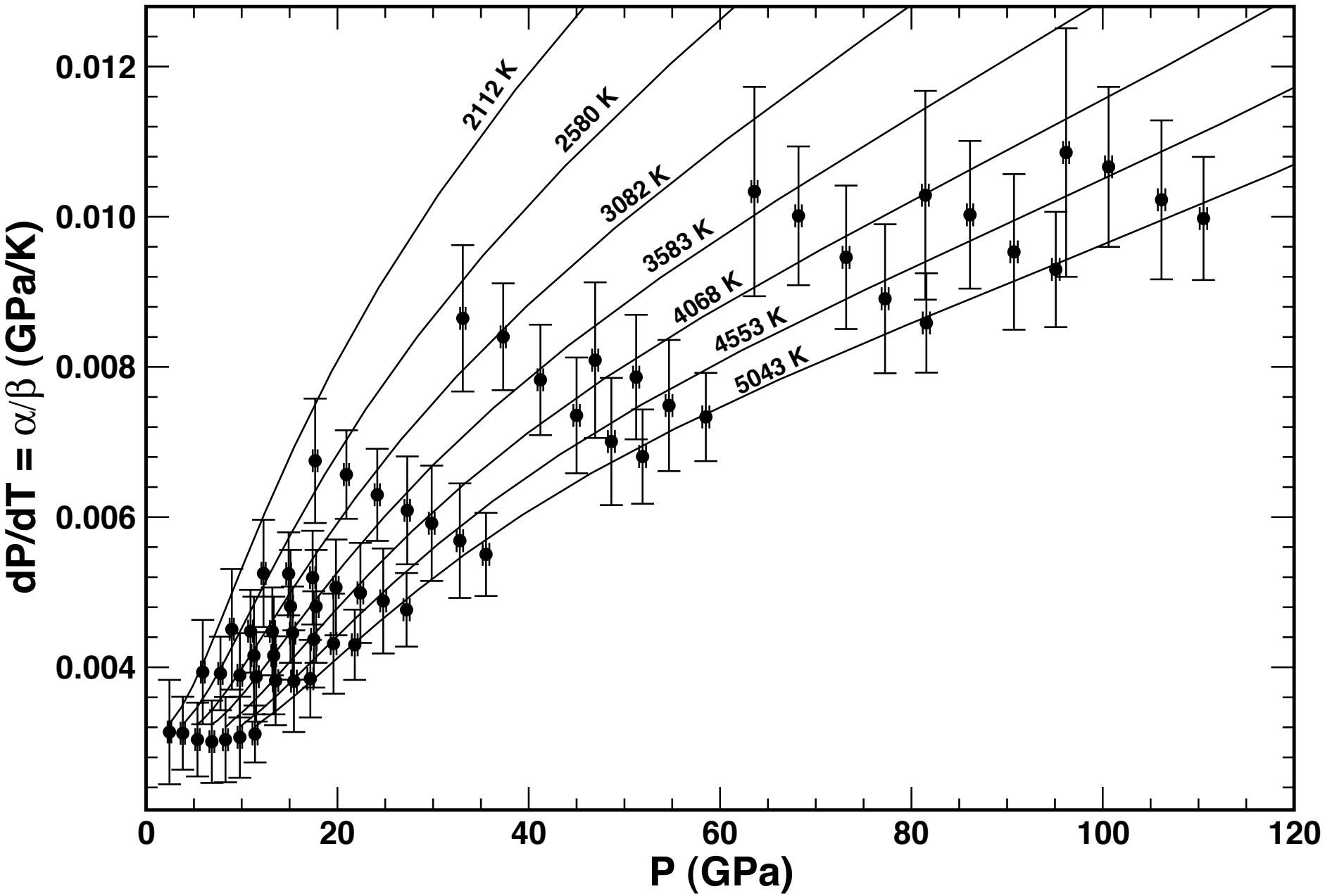
2112 K
2580 K
3082 K
3583 K
4068 K
4553 K
5043 K
0.012
0.010
0.008
0.006
0.004
dP/dT = α/β (GPa/K)
0
20
40
60
80
100
120
P (GPa)

(a.)

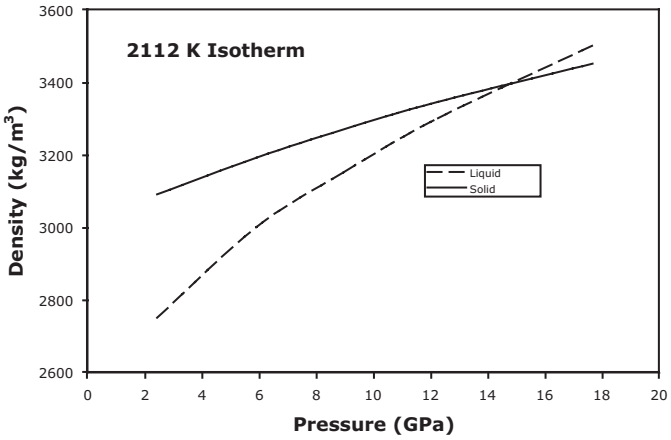
2112 K Isotherm
Density (kg/m3)
Pressure (GPa)
Liquid
Solid
3600
3400
3200
3000
2800
2600
0
2
4
6
8
10
12
14
16
18
20

(b.)

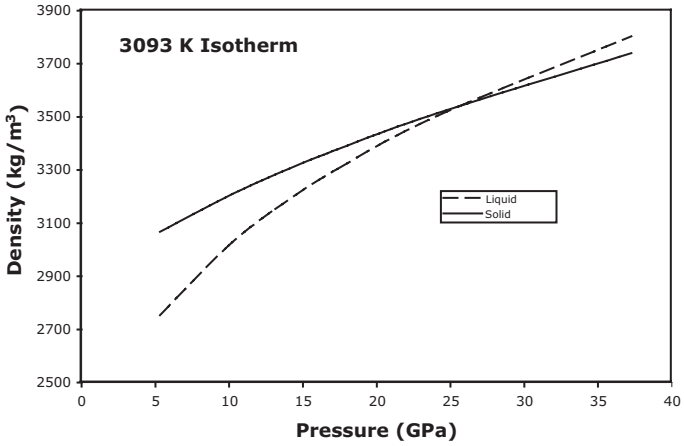
3093 K Isotherm
Density (kg/m3)
Pressure (GPa)
Liquid
Solid
3900
3700
3500
3300
3100
2900
2700
2500
0
5
10
15
20
25
30
35
40

(c.)

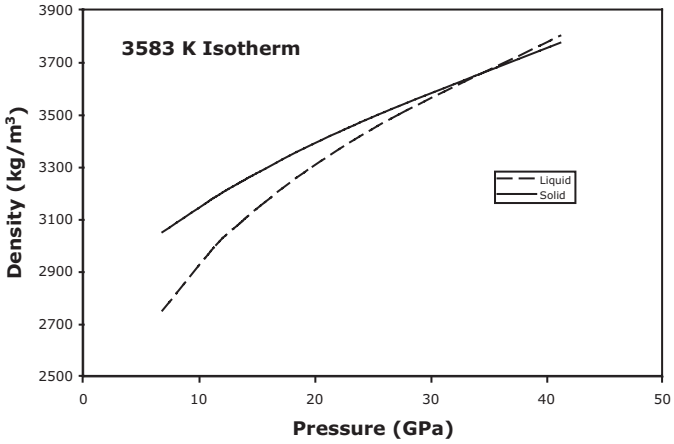
3583 K Isotherm
Density (kg/m3)
Pressure (GPa)
Liquid
Solid
3900
3700
3500
3300
3100
2900
2700
2500
0
10
20
30
40
50

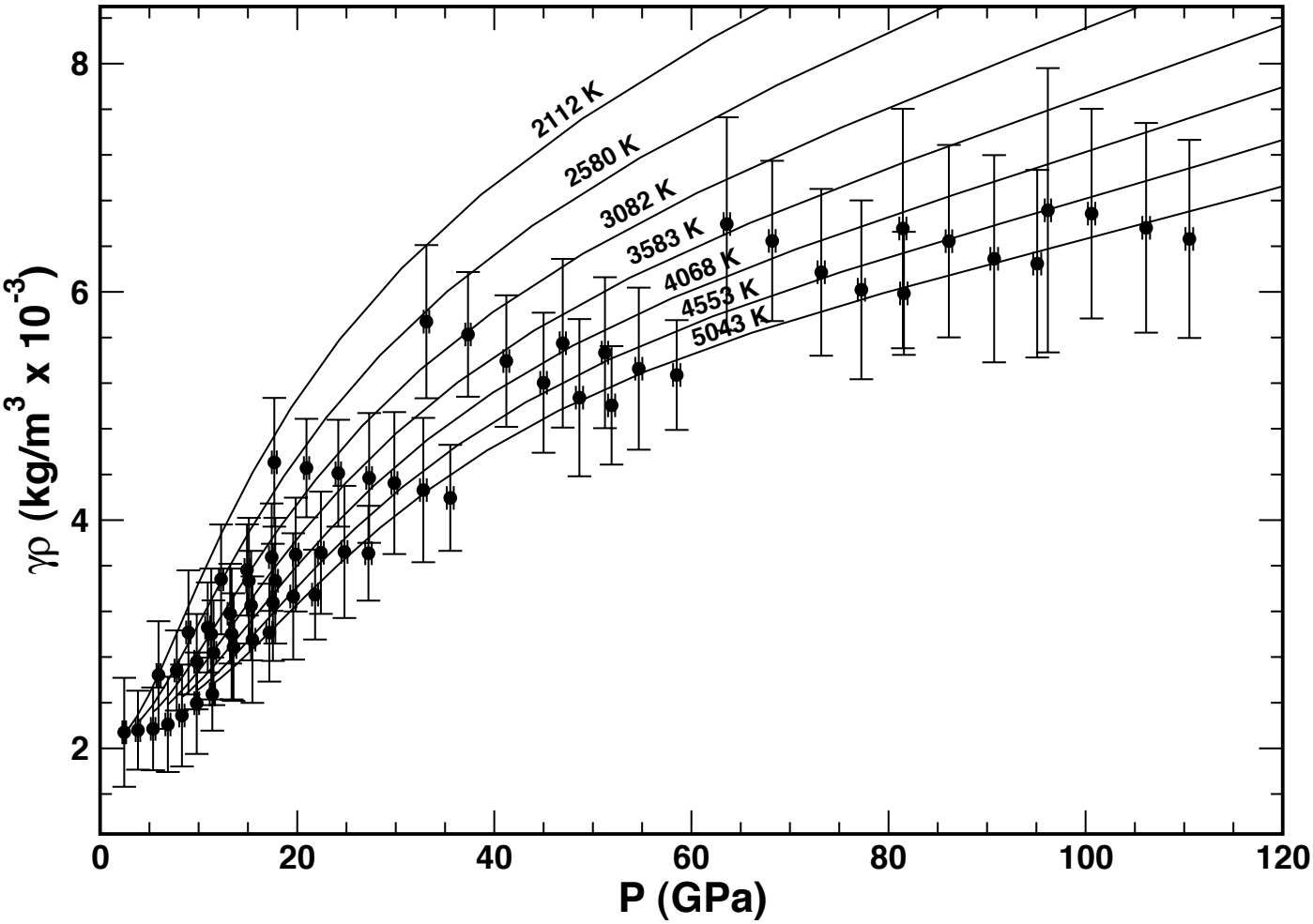
2112 K
2580 K
3082 K
3583 K
4068 K
4553 K
5043 K
γρ (kg/m3 x 10-3)
P (GPa)
0
20
40
60
80
100
120
2
4
6
8

(a.)

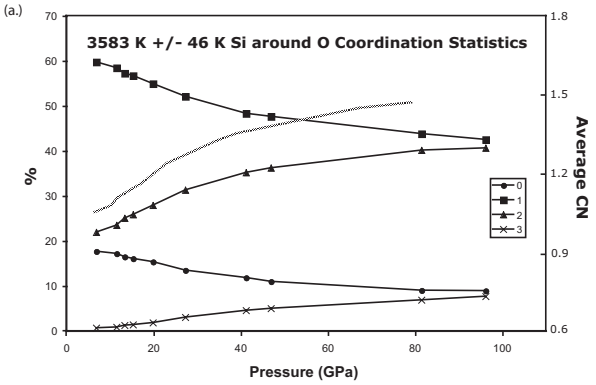
3583 K +/- 46 K Si around O Coordination Statistics
%
Average CN
Pressure (GPa)
0
1
2
3

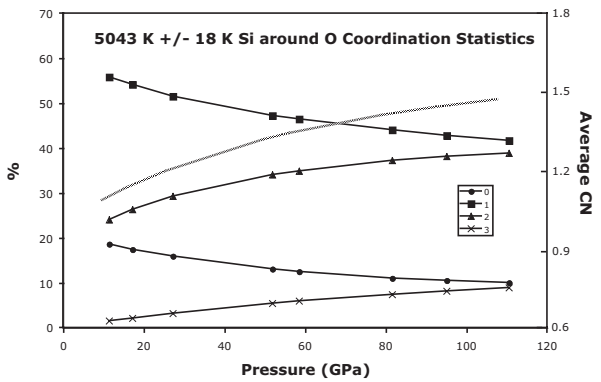
5043 K +/- 18 K Si around O Coordination Statistics
%
Average CN
Pressure (GPa)
0
1
2
3

(b.)

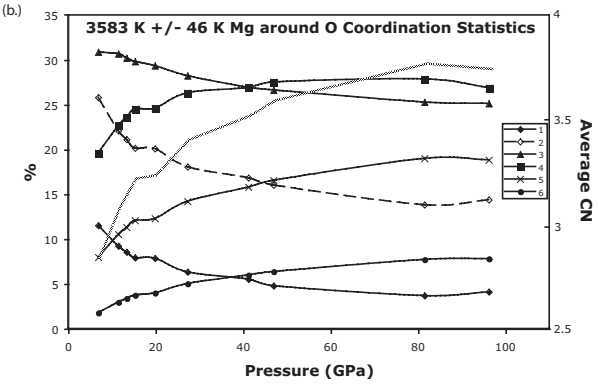
3583 K +/- 46 K Mg around O Coordination Statistics
%
Average CN
Pressure (GPa)
1
2
3
4
5
6

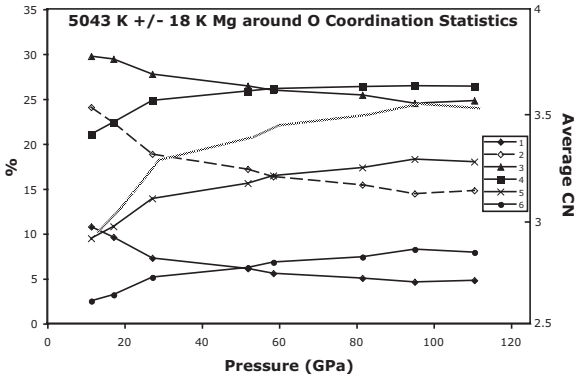
5043 K +/- 18 K Mg around O Coordination Statistics
%
Average CN
Pressure (GPa)
1
2
3
4
5
6

(c.)

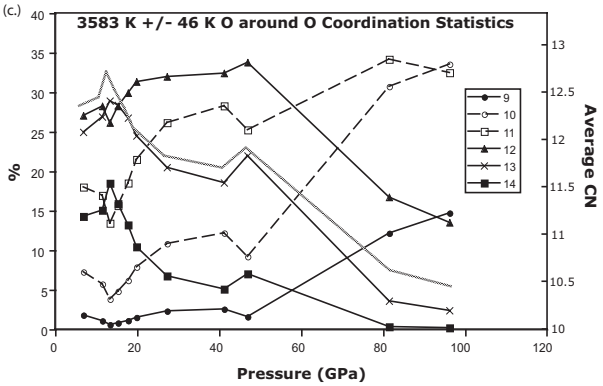
3583 K +/- 46 K O around O Coordination Statistics
%
Average CN
Pressure (GPa)
9
10
11
12
13
14

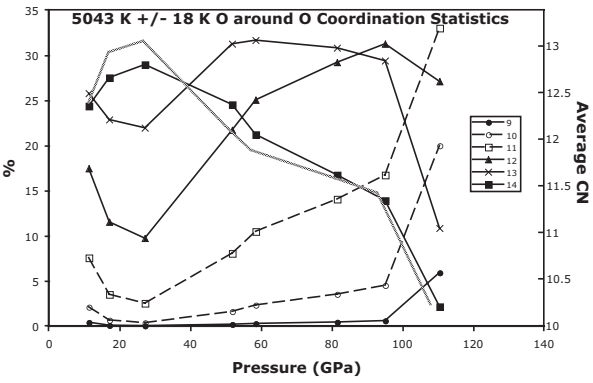
5043 K +/- 18 K O around O Coordination Statistics
%
Average CN
Pressure (GPa)
9
10
11
12
13
14

(a.)

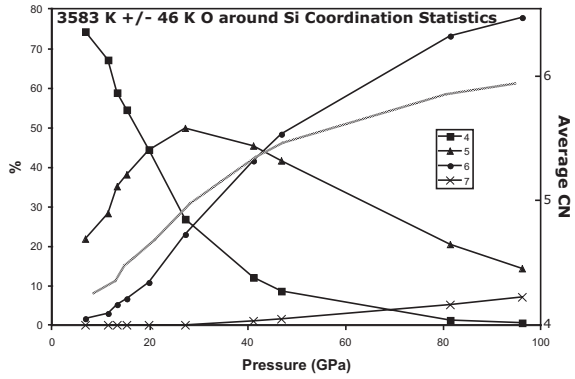
3583 K +/- 46 K O around Si Coordination Statistics
%
Average CN
Pressure (GPa)
4
5
6
7

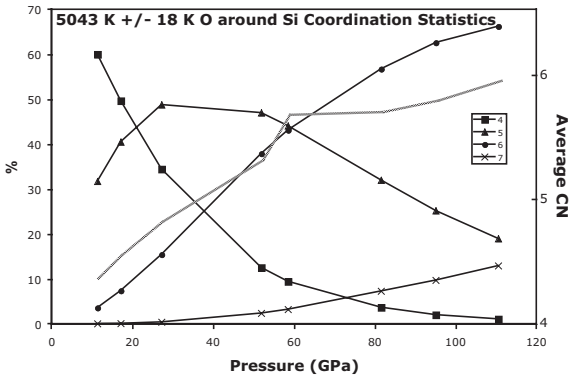
5043 K +/- 18 K O around Si Coordination Statistics
%
Average CN
Pressure (GPa)
4
5
6
7

(b.)

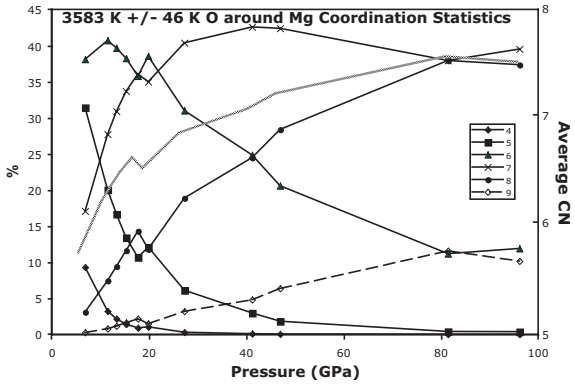
3583 K +/- 46 K O around Mg Coordination Statistics
%
Average CN
Pressure (GPa)
4
5
6
7
8
9

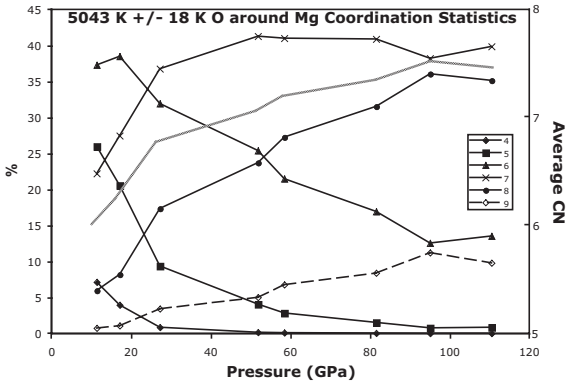
5043 K +/- 18 K O around Mg Coordination Statistics
%
Average CN
Pressure (GPa)
4
5
6
7
8
9

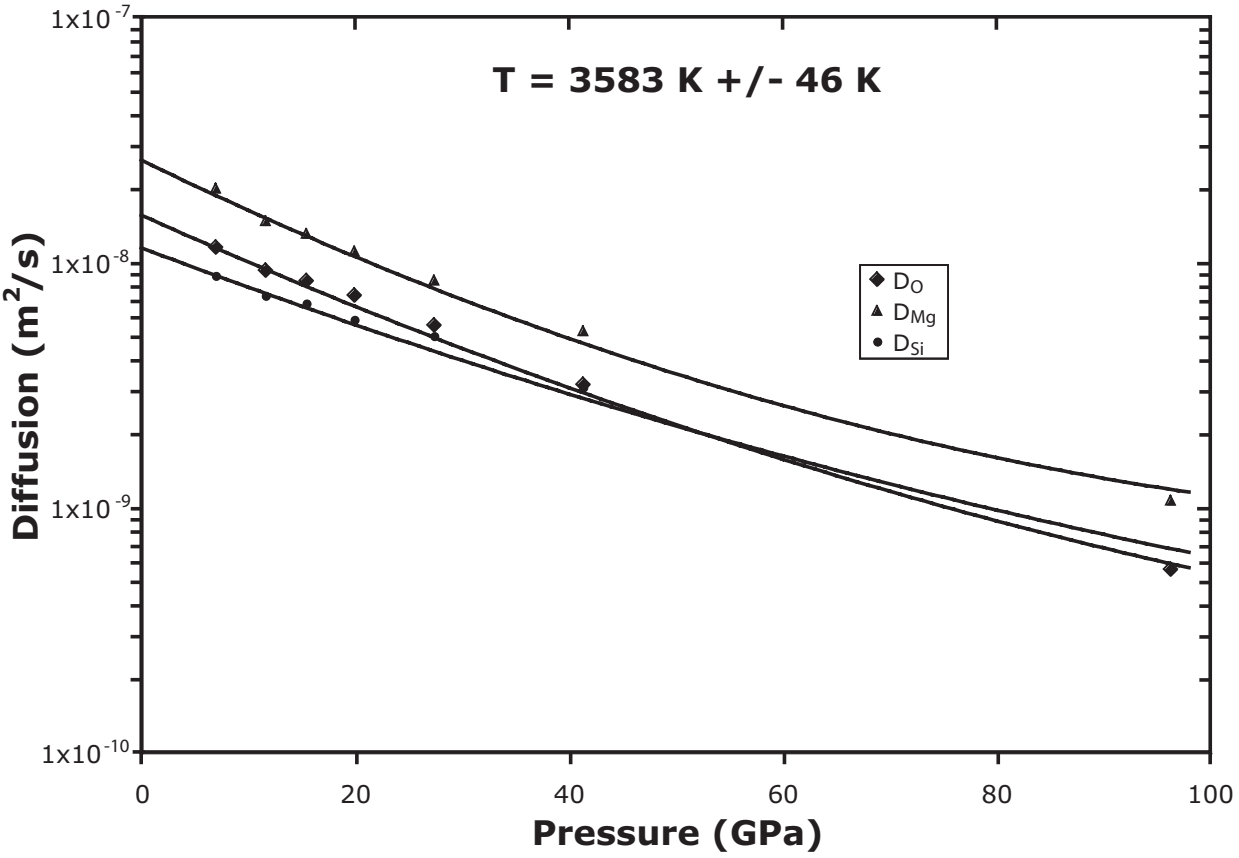
T = 3583 K +/- 46 K
Diffusion (m²/s)
1x10⁻⁷
1x10⁻⁸
1x10⁻⁹
1x10⁻¹⁰
0
20
40
60
80
100
Pressure (GPa)
D_O
D_Mg
D_Si

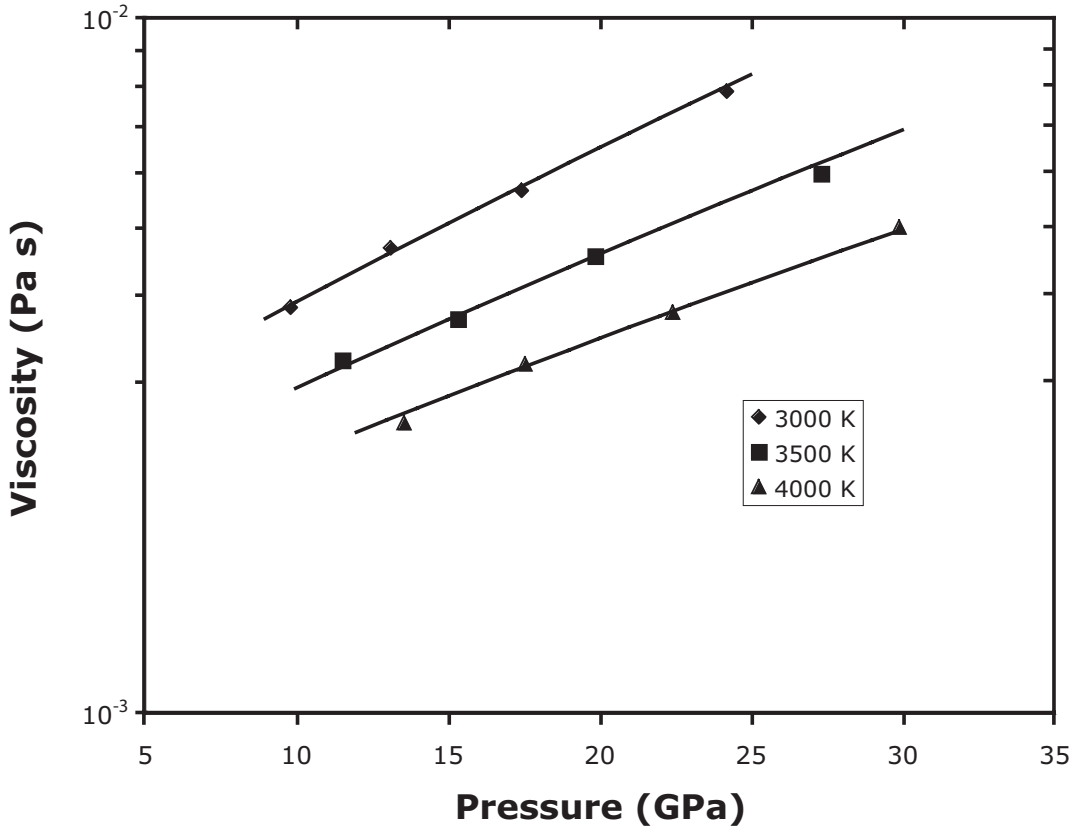
10^{-2}
10^{-3}
Viscosity (Pa s)
5
10
15
20
25
30
35
Pressure (GPa)
3000 K
3500 K
4000 K

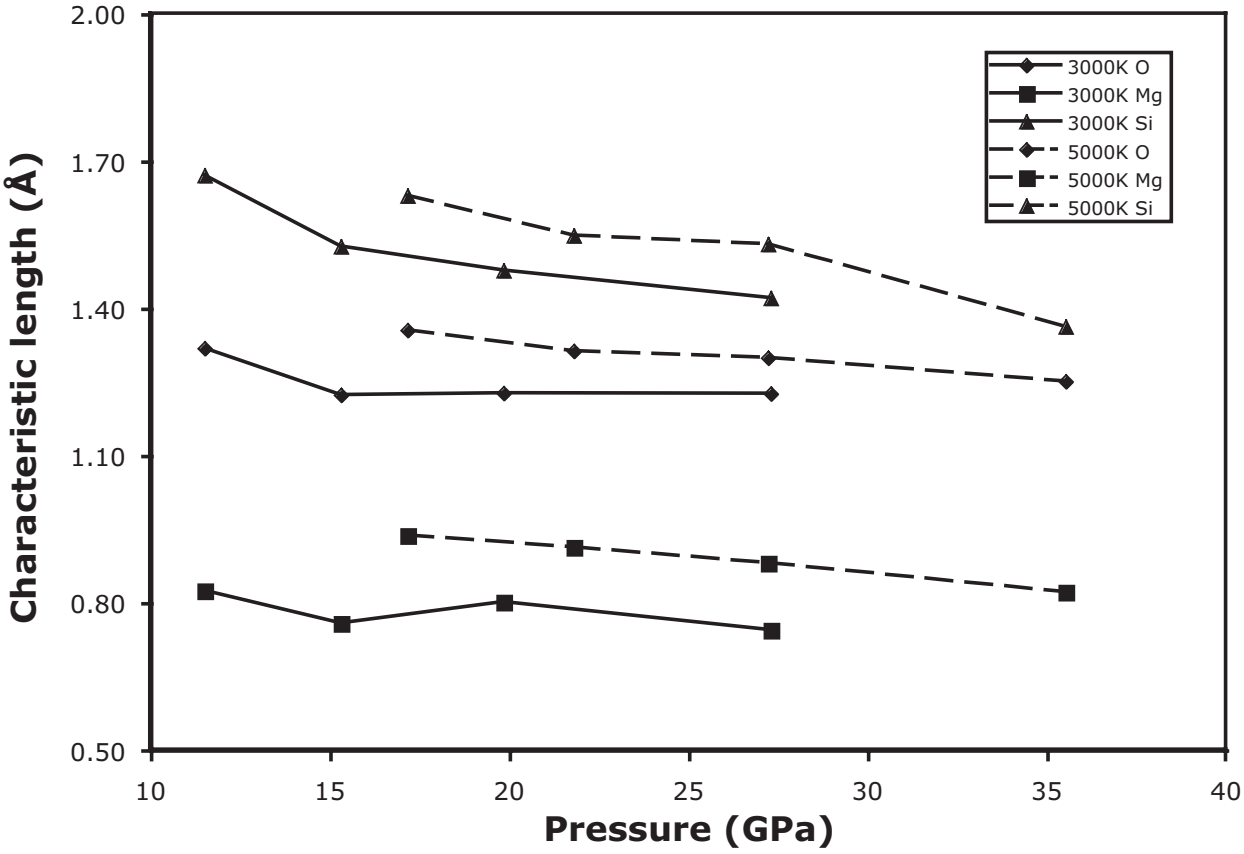
2.00
1.70
1.40
1.10
0.80
0.50
Characteristic length (Å)
10
15
20
25
30
35
40
Pressure (GPa)
3000K O
3000K Mg
3000K Si
5000K O
5000K Mg
5000K Si

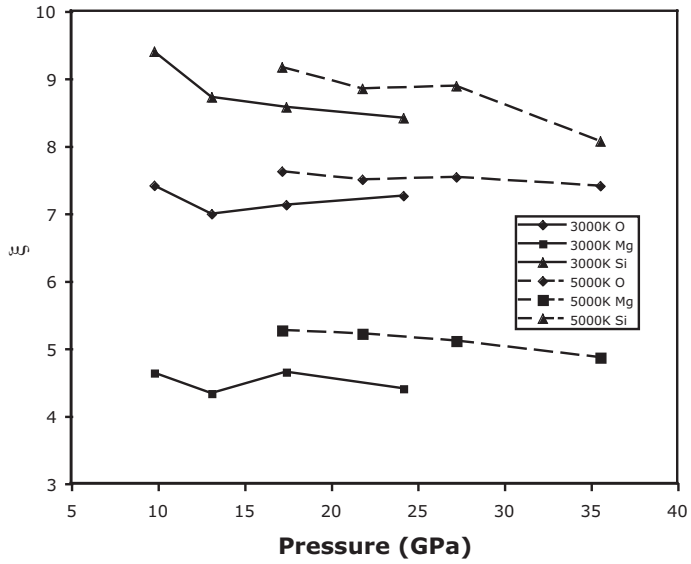
10
9
8
7
6
5
4
3
5
10
15
20
25
30
35
40
Pressure (GPa)
3000K O
3000K Mg
3000K Si
5000K O
5000K Mg
5000K Si

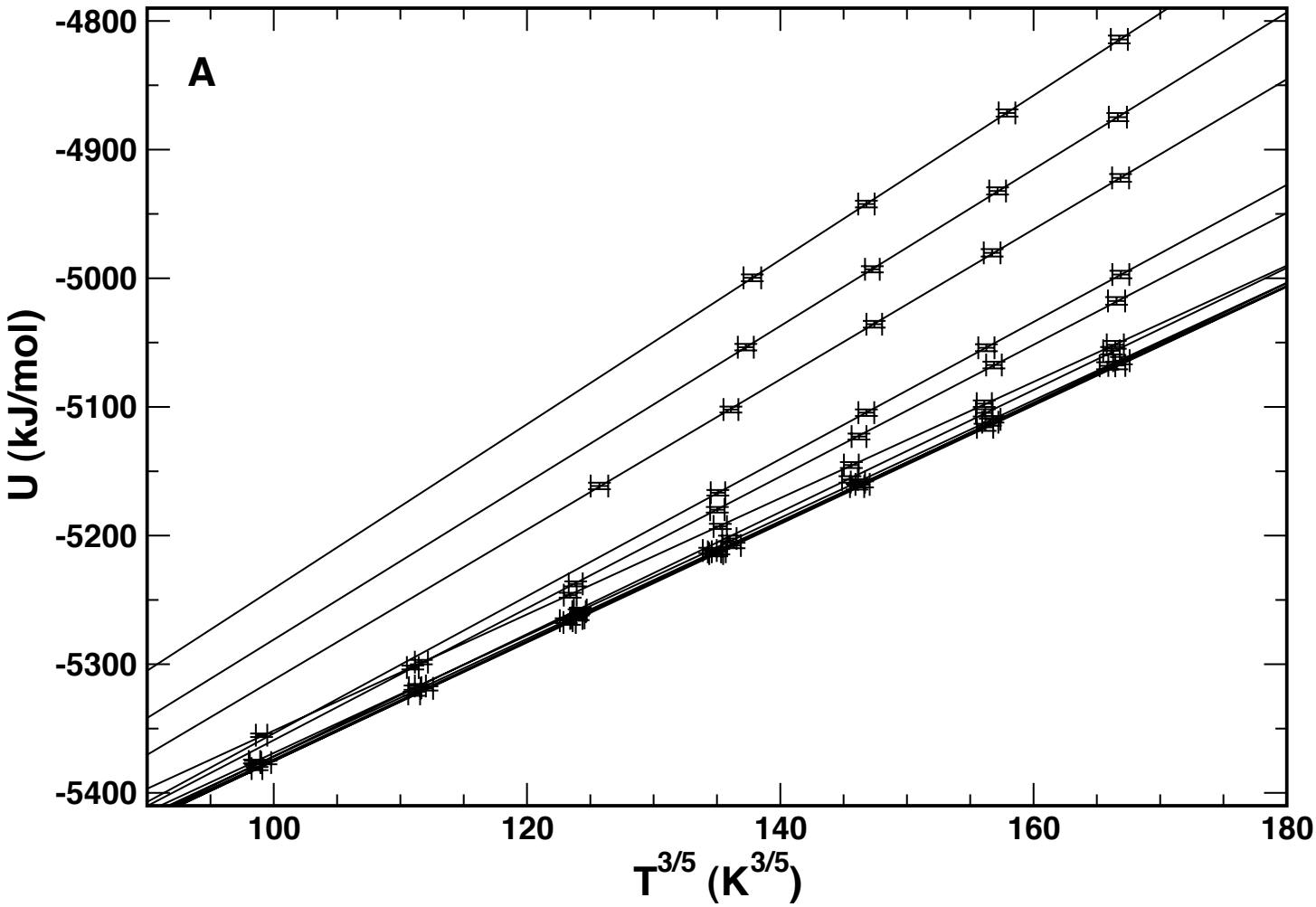
A
-4800
-4900
-5000
-5100
-5200
-5300
-5400
U (kJ/mol)
100
120
140
160
180
T3/5 (K3/5)

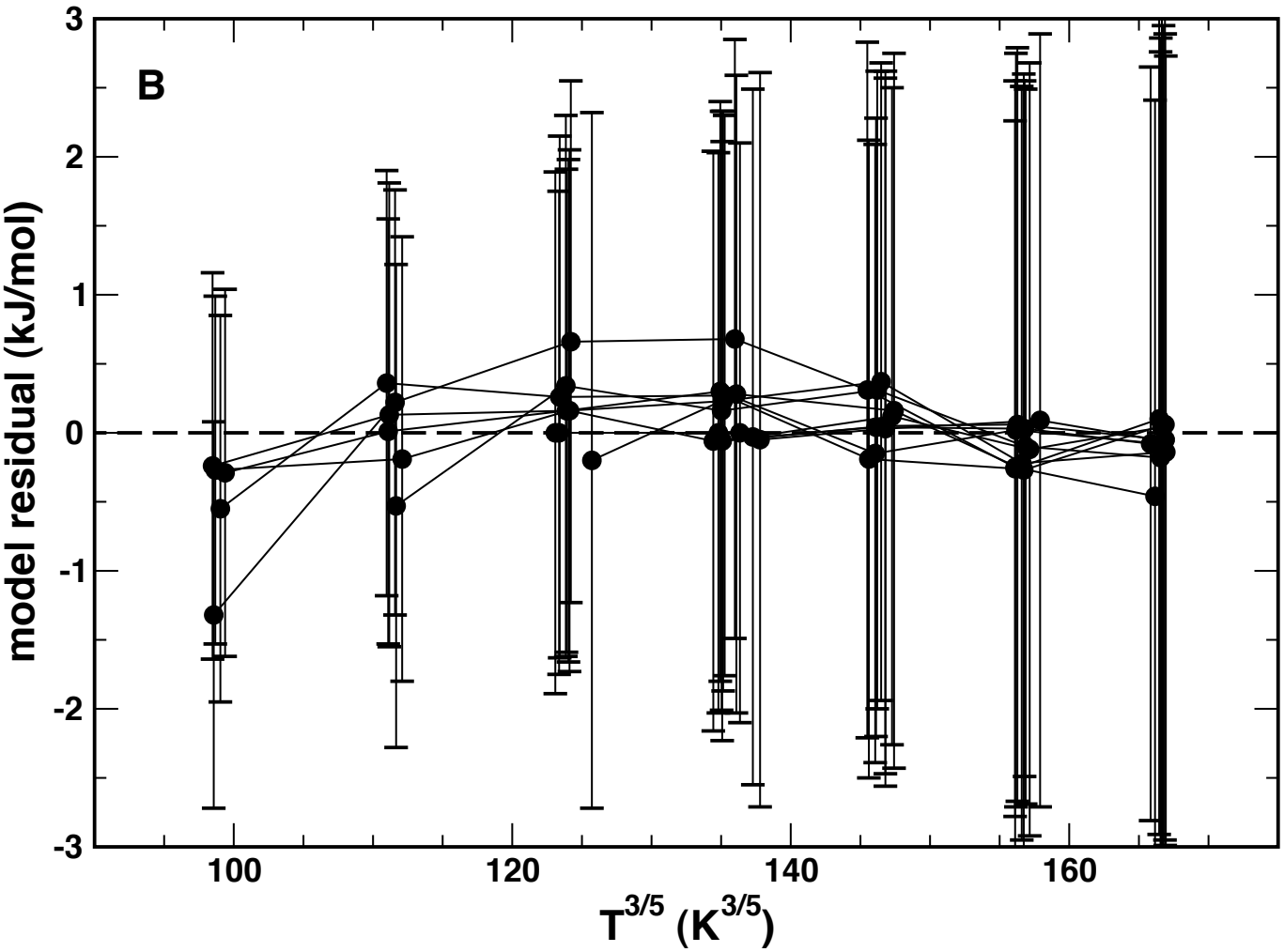
B
model residual (kJ/mol)
3
2
1
0
-1
-2
-3
100
120
140
160
T3/5 (K3/5)

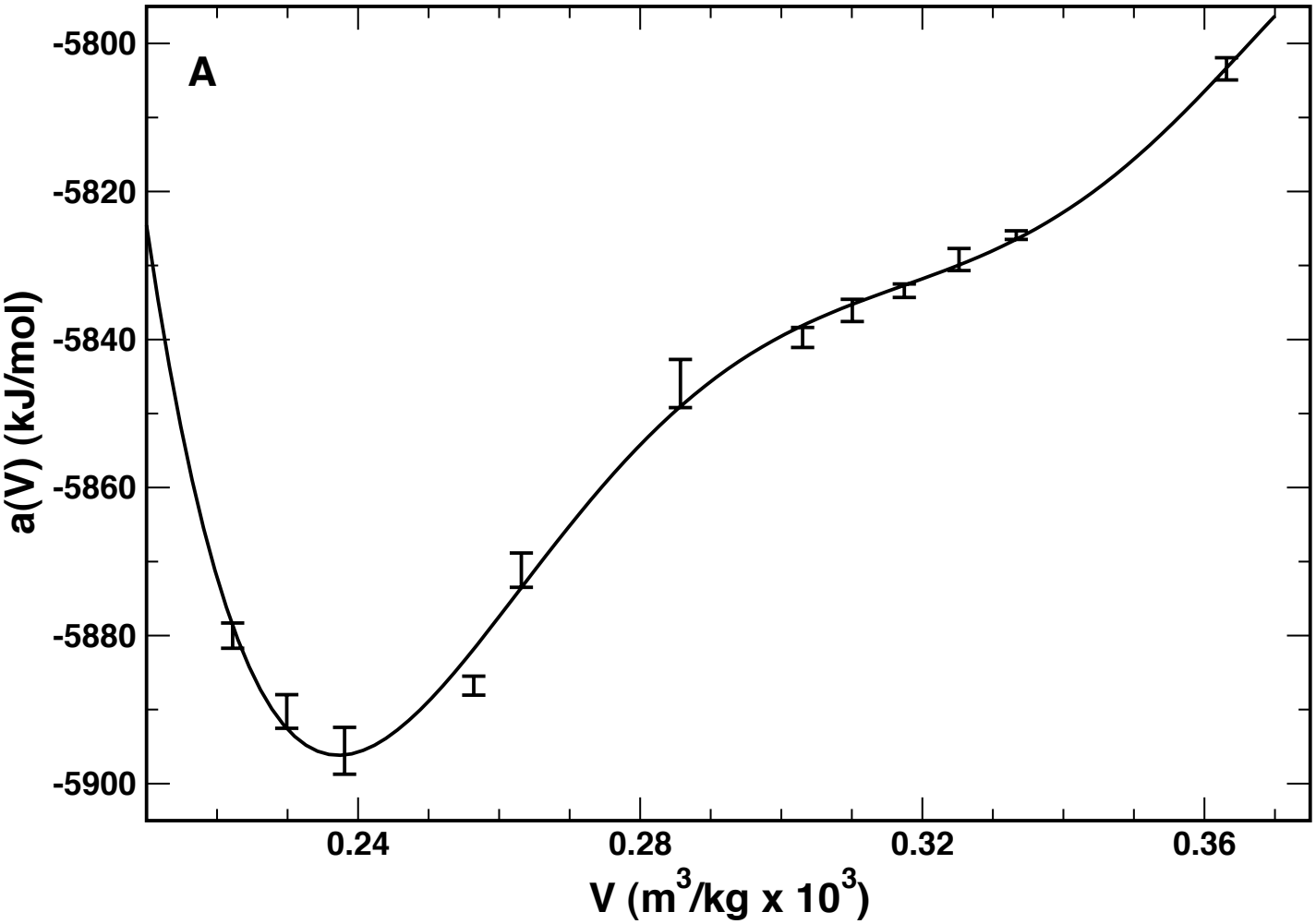
A
-5800
-5820
-5840
-5860
-5880
-5900
a(V) (kJ/mol)
0.24
0.28
0.32
0.36
V (m3/kg x 103)

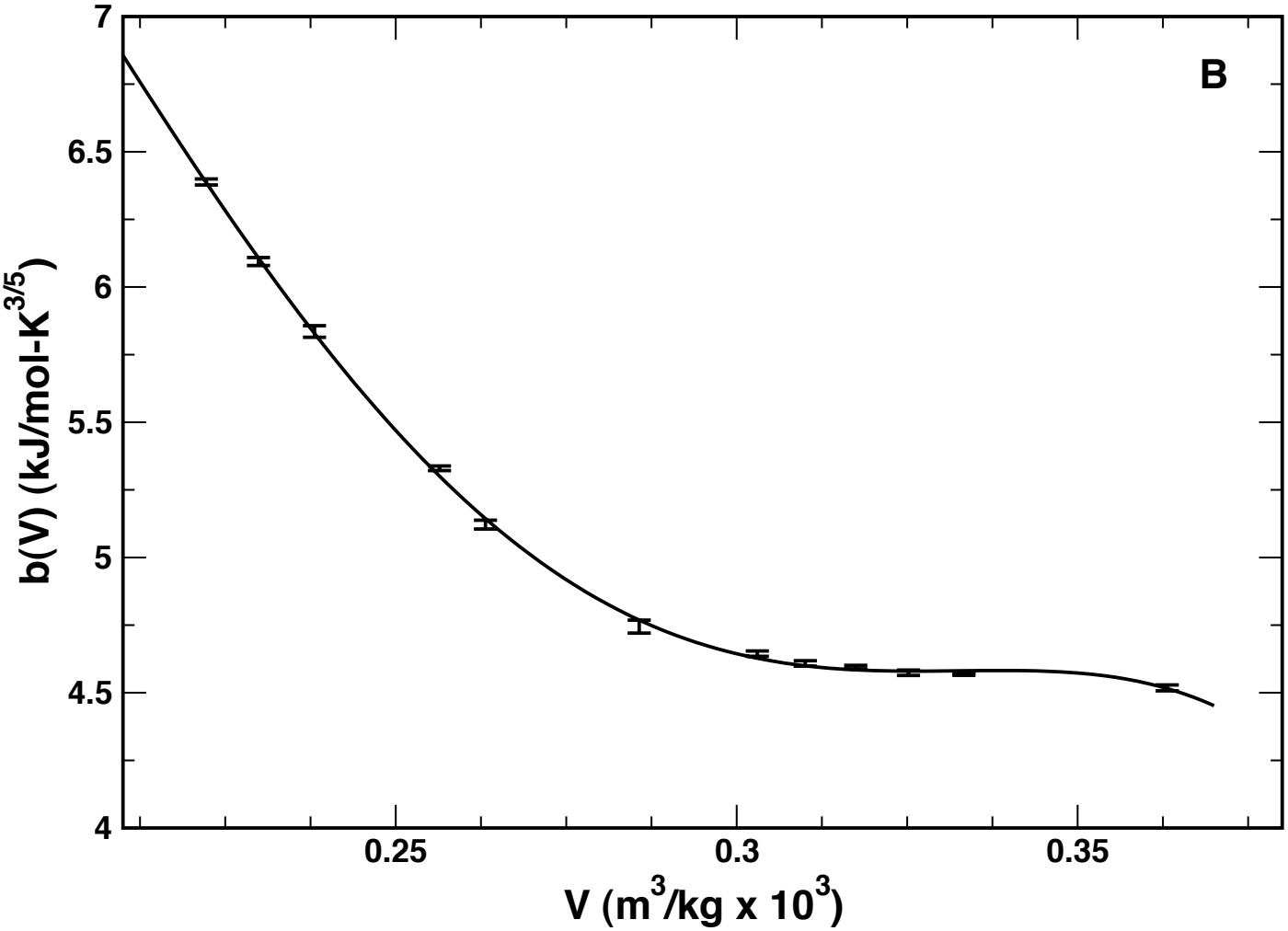
B
7
6.5
6
5.5
5
4.5
4
0.25
0.3
0.35
b(V) (kJ/mol-K^3/5)
V (m^3/kg x 10^3)

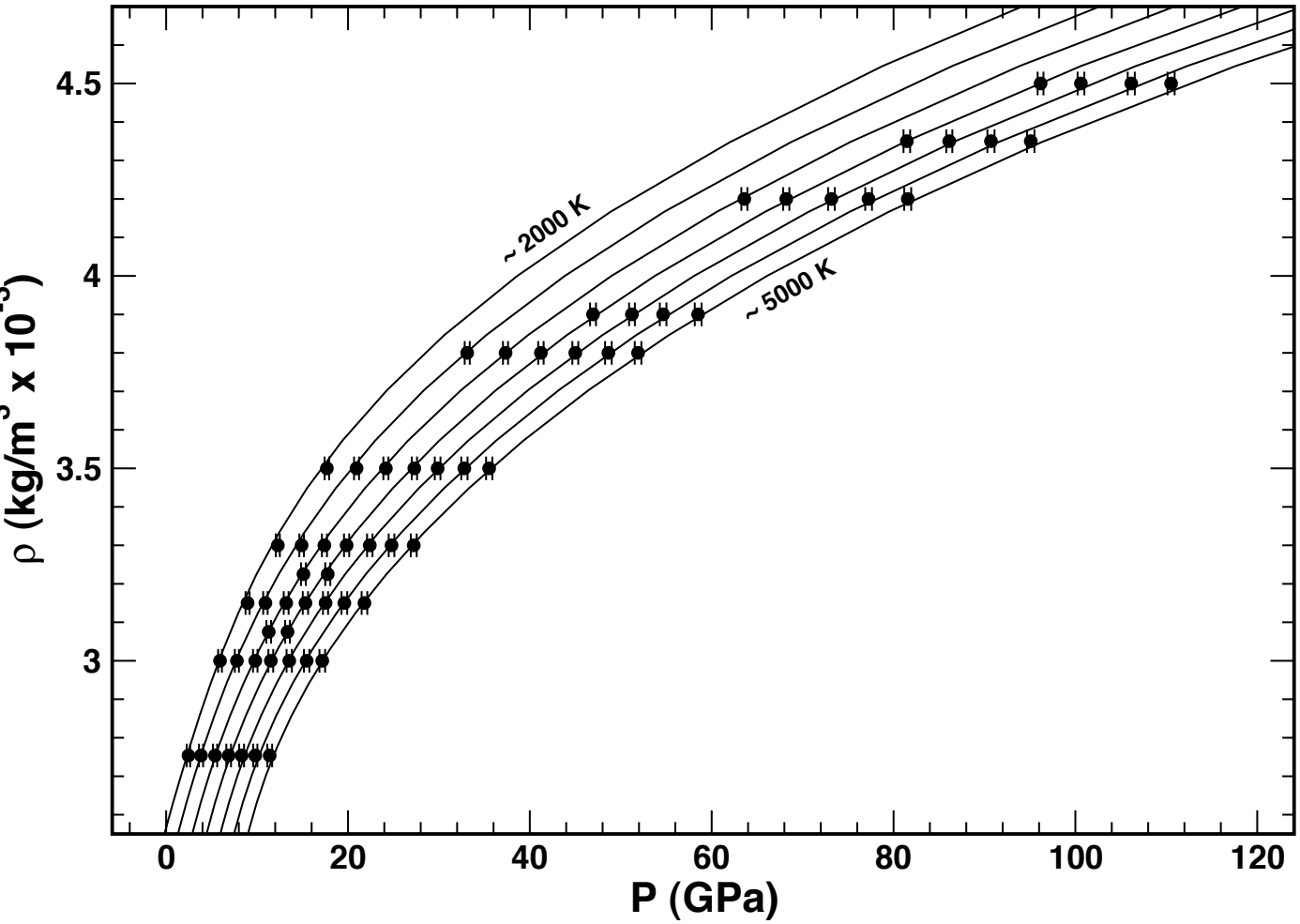
4.5
4
3.5
3
ρ (kg/m3 x 10-3)
0
20
40
60
80
100
120
P (GPa)
~ 2000 K
~ 5000 K

Atom Pair	A (kJ/mol)	B (nm)	C(kJ*nm/mol)
Mg-Mg	7.12E+09	0.80	8.44E+03
Mg-Si	1.48E+11	0.63	1.43E+04
Mg-O	1.32E+07	1.78	2.63E+04
Si-Si	3.23E+13	0.46	2.43E+04
Si-O	2.03E+07	1.61	4.47E+04
O-O	2.61E+06	2.76	8.21E+04

Table 1. Parameters used to define the potential energy pairwise interactions given in text eq (1). The values are from Matsui (1994, 1998)

	Density (kg/m^3)	Temperature (K)	σ_T	Pressure (GPa)	σ_P	U_K (J/mol)	σ_{UK}
MF-1	2753.832	2120	16	2.45	0.19	185220	1400
MF-2	2753.832	2563	18	3.84	0.23	223930	1540
MF-3	2753.832	3059	21	5.38	0.23	267190	1890
MF-4	2753.832	3564	23	6.88	0.26	311290	2030
MF-5	2753.832	4030	27	8.3	0.27	352030	2310
MF-6	2753.832	4526	29	9.8	0.24	395360	2520
MF-7	2753.832	5037	34	11.39	0.27	439950	2940
MF-8	3000.07	2100	16	5.93	0.21	183400	1400
MF-9	3000.07	2570	19	7.78	0.23	224490	1680
MF-10	3000.07	3088	22	9.8	0.25	269710	1890
MF-11	3000.07	3528	24	11.51	0.27	308210	2100
MF-12	3000.07	4054	26	13.54	0.29	354130	2240
MF-13	3000.07	4559	29	15.45	0.3	398230	2520
MF-14	3000.07	5006	31	17.17	0.31	437290	2730
MF-15	3075.071	3046	21	11.28	0.26	266070	1890
MF-16	3075.071	3544	23	13.35	0.26	309540	2030
MF-19	3150.073	2132	15	8.96	0.22	186200	1330
MF-20	3150.073	2567	18	10.92	0.25	224210	1540
MF-21	3150.073	3079	20	13.2	0.27	268940	1750
MF-22	3150.073	3550	24	15.32	0.29	310100	2100
MF-23	3150.073	4051	26	17.53	0.28	353850	2240
MF-24	3150.073	4529	31	19.6	0.31	395640	2730
MF-25	3150.073	5043	34	21.81	0.31	440510	2940
MF-17	3225.075	3057	20	15.1	0.27	267050	1750
MF-18	3225.075	3612	24	17.77	0.28	315490	2100
MF-26	3300.077	2107	15	12.28	0.22	184030	1260
MF-27	3300.077	2606	19	14.9	0.25	227640	1610
MF-28	3300.077	3085	21	17.41	0.28	269500	1820

MF-29	3300.077	3559	24	19.85	0.29	310870	2100
MF-30	3300.077	4071	26	22.4	0.3	355600	2310
MF-31	3300.077	4549	31	24.79	0.31	397320	2730
MF-32	3300.077	5061	33	27.23	0.33	442050	2870
MF-33	3500.081	2103	16	17.68	0.25	183680	1400
MF-34	3500.081	2586	17	20.94	0.27	225890	1540
MF-35	3500.081	3092	21	24.17	0.28	270060	1820
MF-36	3500.081	3596	25	27.3	0.29	314090	2170
MF-37	3500.081	4025	29	29.86	0.31	351610	2520
MF-38	3500.081	4526	32	32.8	0.34	395360	2800
MF-39	3500.081	5022	33	35.53	0.35	438620	2870
MF-40	3800.088	2589	20	33.11	0.28	226170	1750
MF-41	3800.088	3077	23	37.33	0.28	268730	1960
MF-42	3800.088	3554	25	41.22	0.3	310450	2170
MF-43	3800.088	4058	27	45	0.33	354480	2310
MF-44	3800.088	4563	30	48.64	0.37	398580	2590
MF-45	3800.088	5042	34	51.9	0.36	440440	2940
MF-46	3900.091	3556	25	46.95	0.32	310590	2170
MF-47	3900.091	4085	29	51.23	0.32	356860	2520
MF-48	3900.091	4534	31	54.66	0.36	395990	2730
MF-49	3900.091	5059	34	58.51	0.37	441910	2940
MF-50	4200.098	3155	29	63.59	0.33	275590	2310
MF-51	4200.098	3601	26	68.2	0.34	314580	2310
MF-52	4200.098	4114	29	73.17	0.36	359380	2590
MF-53	4200.098	4556	32	77.25	0.37	398790	2800
MF-54	4200.098	5058	34	81.56	0.38	441770	3010
MF-55	4350.101	3653	28	81.46	0.36	319060	2520
MF-56	4350.101	4107	27	86.13	0.33	358750	2380
MF-57	4350.101	4577	32	90.72	0.39	399840	2800
MF-58	4350.101	5047	36	95.09	0.41	440860	3150

MF-59	4500.104	3193	36	90.78	0.33	278950	3150
MF-60	4500.104	3676	31	96.17	0.32	321090	2660
MF-61	4500.104	4085	30	100.61	0.37	356790	2590
MF-62	4500.104	4613	32	106.14	0.39	402920	2800
MF-63	4500.104	5053	34	110.53	0.39	441350	3010

U_P (J/mol)	Δ_{UP}	U (J/mol)	D_{Oxygen} (m^2/s)	$D_{Magnesium}$ (m^2/s)	$D_{Silicon}$ (m^2/s)
-5355210	1400	-5169990	2.37434E-09	5.856E-09	1.74043E-09
-5302570	1540	-5078640	4.65097E-09	9.6692E-09	3.3592E-09
-5246360	1890	-4979170	7.59916E-09	1.43174E-08	5.52539E-09
-5192880	2030	-4881590	1.16015E-08	2.0195E-08	8.89266E-09
-5145140	2310	-4793110	1.4905E-08	2.47545E-08	1.14544E-08
-5097470	2520	-4702110	1.84103E-08	2.90117E-08	1.50583E-08
-5051690	3010	-4611740	2.28607E-08	3.41309E-08	1.80698E-08
-5375650	1400	-5192250	1.79283E-09	3.75576E-09	1.30934E-09
-5318250	1680	-5093760	3.77774E-09	6.99033E-09	2.7972E-09
-5259170	1890	-4989390	6.697E-09	1.07029E-08	5.28175E-09
-5211570	2100	-4903360	9.33912E-09	1.48319E-08	7.36443E-09
-5158370	2240	-4804240	1.20133E-08	1.98142E-08	9.5647E-09
-5109650	2520	-4711350	1.57584E-08	2.38756E-08	1.27229E-08
-5068000	2730	-4631060	1.901E-08	2.74967E-08	1.58046E-08
-5266170	1890	-5000100	6.09734E-09	9.731E-09	4.87107E-09
-5212620	2030	-4903080	8.39825E-09	1.40528E-08	6.54406E-09
-5376420	1330	-5190220	1.62793E-09	2.3748E-09	1.29742E-09
-5323010	1540	-5098800	3.44473E-09	6.12514E-09	2.69043E-09
-5264420	1750	-4995480	5.92494E-09	9.55997E-09	4.74721E-09
-5214020	2100	-4903920	8.45518E-09	1.31835E-08	6.84507E-09
-5161940	2240	-4808090	1.1062E-08	1.67539E-08	9.10913E-09
-5115880	2730	-4720240	1.38519E-08	2.11272E-08	1.1851E-08
-5067790	2940	-4627350	1.72488E-08	2.47995E-08	1.46251E-08
-5267570	1750	-5000520	5.27954E-09	8.62037E-09	4.11291E-09
-5207720	2100	-4892230	8.22271E-09	1.23452E-08	6.50486E-09
-5381110	1260	-5197080	1.22553E-09	2.23464E-09	9.61157E-10
-5318810	1610	-5091170	2.91619E-09	4.9308E-09	2.36622E-09
-5263930	1820	-4994430	4.88279E-09	7.47756E-09	4.05582E-09

-5212550	2100	-4901680	7.38812E-09	1.11809E-08	5.86429E-09
-5160190	2310	-4804590	9.49402E-09	1.42129E-08	8.07368E-09
-5111890	2730	-4714500	1.22461E-08	1.83887E-08	1.06377E-08
-5064010	2870	-4621960	1.49849E-08	2.20943E-08	1.27091E-08
-5376490	1400	-5192810	7.77496E-10	1.44093E-09	6.61869E-10
-5316920	1540	-5091030	1.95231E-09	3.2983E-09	1.65602E-09
-5257910	1890	-4987850	3.51512E-09	5.7942E-09	3.03384E-09
-5202260	2170	-4888170	5.5737E-09	8.50932E-09	5.03701E-09
-5156410	2520	-4804800	7.8508E-09	1.16736E-08	7.11607E-09
-5104610	2800	-4709250	9.59463E-09	1.4458E-08	8.66701E-09
-5056310	2870	-4617690	1.21876E-08	1.85475E-08	1.11875E-08
-5298370	1750	-5072200	7.70673E-10	1.45983E-09	7.16035E-10
-5237540	1960	-4968740	1.81712E-09	3.13485E-09	1.73061E-09
-5179930	2170	-4869480	3.19707E-09	5.27668E-09	3.11389E-09
-5123020	2310	-4768540	4.94357E-09	8.10076E-09	4.65333E-09
-5067440	2590	-4668860	7.22413E-09	1.11791E-08	6.94853E-09
-5017600	2940	-4577230	8.76232E-09	1.34333E-08	8.30179E-09
-5166700	2170	-4856110	2.71912E-09	4.52492E-09	2.5594E-09
-5104470	2520	-4747610	4.40976E-09	6.79567E-09	4.26699E-09
-5054000	2730	-4657940	6.01444E-09	9.08077E-09	5.81759E-09
-4997090	2940	-4555180	7.6954E-09	1.18325E-08	7.47301E-09
-5161450	2520	-4885790	5.09156E-10	1.03267E-09	5.41261E-10
-5102020	2310	-4787440	1.29297E-09	2.35794E-09	1.30096E-09
-5035730	2590	-4676350	2.48618E-09	4.15517E-09	2.46047E-09
-4980220	2870	-4581430	3.61264E-09	6.19124E-09	3.70026E-09
-4921980	3010	-4480140	5.49525E-09	8.45422E-09	5.61051E-09
-5053580	2520	-4734520	8.79399E-10	1.61576E-09	8.97028E-10
-4993030	2380	-4634280	1.85002E-09	3.01008E-09	1.86094E-09
-4932130	2800	-4532290	3.12685E-09	5.00619E-09	3.09932E-09
-4874730	3150	-4433870	4.18775E-09	6.4165E-09	4.31377E-09

-5064710	3150	-4785760	1.14329E-10	3.3152E-10	1.37657E-10
-4999610	2660	-4678520	4.96024E-10	1.07583E-09	5.63635E-10
-4942280	2590	-4585490	1.12865E-09	3.14279E-09	1.19913E-09
-4871510	2800	-4468590	2.34535E-09	3.79356E-09	2.38497E-09
-4814390	3010	-4373040	3.55809E-09	5.56731E-09	3.61505E-09

	Density (kg/m^3)	Temperature (K)	Pressure (GPa)	Thermal Pressure (GPa/K)	$_{Th}P$
MF-1	2753.832	2120	2.45	0.003137698	0.000694696
MF-2	2753.832	2563	3.84	0.003121268	0.000485446
MF-3	2753.832	3059	5.38	0.003037568	0.000491449
MF-4	2753.832	3564	6.88	0.003008754	0.000549284
MF-5	2753.832	4030	8.3	0.003035702	0.000567805
MF-6	2753.832	4526	9.8	0.00306787	0.000539127
MF-7	2753.832	5037	11.39	0.003111546	0.000378752
MF-8	3000.07	2100	5.93	0.00393617	0.000694541
MF-9	3000.07	2570	7.78	0.003917892	0.000489988
MF-10	3000.07	3088	9.8	0.003892989	0.000561258
MF-11	3000.07	3528	11.51	0.00387284	0.000595174
MF-12	3000.07	4054	13.54	0.003820747	0.000592161
MF-13	3000.07	4559	15.45	0.003815026	0.000676884
MF-14	3000.07	5006	17.17	0.003847875	0.000515975
MF-15	3075.071	3046	11.28	0.004156627	0.00078277
MF-16	3075.071	3544	13.35	0.004156627	0.00078277
MF-17	3150.073	2132	8.96	0.004505747	0.000803104
MF-18	3150.073	2567	10.92	0.004479436	0.00055142
MF-19	3150.073	3079	13.2	0.004477093	0.000584834
MF-20	3150.073	3550	15.32	0.00445612	0.000620748
MF-21	3150.073	4051	17.53	0.004370861	0.000640812
MF-22	3150.073	4529	19.6	0.004315077	0.000665905
MF-23	3150.073	5043	21.81	0.004299611	0.000467874
MF-24	3225.075	3057	15.1	0.004810811	0.00075135
MF-25	3225.075	3612	17.77	0.004810811	0.00075135
MF-26	3300.077	2107	12.28	0.005250501	0.000714323
MF-27	3300.077	2606	14.9	0.005245292	0.000552345
MF-28	3300.077	3085	17.41	0.005193881	0.000623156

MF-29	3300.077	3559	19.85	0.005064074	0.000637538
MF-30	3300.077	4071	22.4	0.004990234	0.000666375
MF-31	3300.077	4549	24.79	0.004882813	0.00069879
MF-32	3300.077	5061	27.23	0.004765625	0.0004898
MF-33	3500.081	2103	17.68	0.006749482	0.000828747
MF-34	3500.081	2586	20.94	0.006566441	0.000590324
MF-35	3500.081	3092	24.17	0.006296858	0.000614143
MF-36	3500.081	3596	27.3	0.006088842	0.000718394
MF-37	3500.081	4025	29.86	0.005917815	0.000768452
MF-38	3500.081	4526	32.8	0.005686148	0.000762777
MF-39	3500.081	5022	35.53	0.005504032	0.00055408
MF-40	3800.088	2589	33.11	0.008647541	0.000974752
MF-41	3800.088	3077	37.33	0.008401339	0.000711965
MF-42	3800.088	3554	41.22	0.007827568	0.000734897
MF-43	3800.088	4058	45	0.00735396	0.000771127
MF-44	3800.088	4563	48.64	0.007006883	0.000847389
MF-45	3800.088	5042	51.9	0.006805846	0.00062781
MF-46	3900.091	3556	46.95	0.008090737	0.001036711
MF-47	3900.091	4085	51.23	0.007864968	0.000828731
MF-48	3900.091	4534	54.66	0.007486266	0.00087355
MF-49	3900.091	5059	58.51	0.007333333	0.000587355
MF-50	4200.098	3155	63.59	0.010336323	0.001394063
MF-51	4200.098	3601	68.2	0.010012216	0.000924144
MF-52	4200.098	4114	73.17	0.009459439	0.000955287
MF-53	4200.098	4556	77.25	0.008908213	0.000991395
MF-54	4200.098	5058	81.56	0.008585657	0.000662179
MF-55	4350.101	3653	81.46	0.010286344	0.001390614
MF-56	4350.101	4107	86.13	0.010026151	0.000983895
MF-57	4350.101	4577	90.72	0.009531915	0.001036323
MF-58	4350.101	5047	95.09	0.009297872	0.000767703

MF-59	4500.104	3193	90.78	0.01115942	0.001435297
MF-60	4500.104	3676	96.17	0.010855746	0.001655771
MF-61	4500.104	4085	100.61	0.010664615	0.001064808
MF-62	4500.104	4613	106.14	0.010225379	0.001058996
MF-63	4500.104	5053	110.53	0.009977273	0.000820396

Beta (GPa^{-1})	Beta	Alpha (K^{-1})	alpha	Cv (J/mol K)	Cv	Gamma	gamma
0.024594804	0.001997815	7.71711E-05	1.82E-05	206.203278	5.60500288	0.7773942	0.17340972
0.021723329	0.001790098	6.78043E-05	1.1934E-05	203.371678	7.91705519	0.78409086	0.12571052
0.019364235	0.001485542	5.88202E-05	1.0532E-05	196.881841	8.17101101	0.78821758	0.13165488
0.018485943	0.001493835	5.56196E-05	1.1104E-05	191.545399	9.36542118	0.80249197	0.15166781
0.016333954	0.00061643	4.9585E-05	9.4614E-06	186.665513	10.2912468	0.83084656	0.16201383
0.015148658	0.001028189	4.64741E-05	8.755E-06	180.154687	10.6534179	0.86999577	0.16131118
0.014807944	0.00105127	4.60756E-05	6.4927E-06	176.845544	7.73271953	0.89889278	0.11626283
0.019460138	0.001335342	7.65984E-05	1.4502E-05	209.548723	5.5373216	0.880888	0.15716695
0.01811534	0.001300599	7.09739E-05	1.0235E-05	205.515457	7.91341941	0.89400473	0.11698736
0.017924008	0.002431013	6.9778E-05	1.3812E-05	198.500374	9.1807489	0.91971583	0.13925284
0.015550178	0.001909742	6.02233E-05	1.1847E-05	191.977802	9.61749482	0.94604183	0.15291646
0.013984309	0.000925372	5.34305E-05	9.0042E-06	186.186859	9.51226827	0.96234565	0.15704452
0.013237343	0.000868174	5.05008E-05	9.5527E-06	181.776264	11.0928901	0.98422008	0.18466652
0.012296219	0.000769702	4.73143E-05	7.0018E-06	179.615857	8.52873359	1.00463451	0.14291155
0.014324563	0.002189036	5.95419E-05	1.444E-05	194.815123	6.09184992	0.97617216	0.18634842
0.012797916	0.001815701	5.31962E-05	1.2543E-05	194.815123	6.09184992	0.97617216	0.18634842
0.014981839	0.001025667	6.75044E-05	1.2889E-05	210.156438	5.65991122	0.95756161	0.1726131
0.013338676	0.000916582	5.97497E-05	8.4236E-06	205.974505	7.75566256	0.97129798	0.12503535
0.01246654	0.001746567	5.58139E-05	1.0691E-05	198.091666	8.34733343	1.0094215	0.13854981
0.010759667	0.001363218	4.79464E-05	9.0284E-06	192.832063	9.33727174	1.03209626	0.15221178
0.010723866	0.000694707	4.68725E-05	7.5129E-06	187.528029	10.3014818	1.04098242	0.16297984
0.010169842	0.000668005	4.38837E-05	7.3601E-06	182.249341	11.2214416	1.05746313	0.17569773
0.009449567	0.000591191	4.06295E-05	5.0998E-06	180.715991	8.08842379	1.06261314	0.12503007
0.011035434	0.001427352	5.30894E-05	1.0766E-05	195.112957	5.49146273	1.07561185	0.17069451
0.010277263	0.001294507	4.9442E-05	9.9202E-06	195.112957	5.49146273	1.07561185	0.17069451
0.0122564	0.000657765	6.43522E-05	9.4116E-06	212.239963	5.14808168	1.05466064	0.14574774
0.010624168	0.000555209	5.57269E-05	6.5511E-06	207.099039	7.88321414	1.07976877	0.12090349
0.009284834	0.000784751	4.82243E-05	7.0774E-06	198.814524	8.88645879	1.1137381	0.14259653

0.009211067	0.00080034	4.66455E-05	7.1352E-06	192.647898	9.28763689	1.12066273	0.15107601
0.008638374	0.000427771	4.31075E-05	6.1395E-06	189.046824	10.3225975	1.12535803	0.16235348
0.008072489	0.000398818	3.94165E-05	5.9676E-06	184.603559	11.2909881	1.12763652	0.1754991
0.007763069	0.000382836	3.69959E-05	4.2174E-06	180.738334	7.99148056	1.12410984	0.12577127
0.010893211	0.0006712	7.35235E-05	1.0101E-05	210.720144	5.09245476	1.28750685	0.16112164
0.007976115	0.000249219	5.23747E-05	4.9848E-06	207.31442	7.45453105	1.27316783	0.12327394
0.007271837	0.00021862	4.57897E-05	4.6733E-06	200.841128	8.40676242	1.26024913	0.13375578
0.00675652	0.00019663	4.11394E-05	4.9993E-06	196.052541	10.7815386	1.24838156	0.16250443
0.006430378	0.000189413	3.80538E-05	5.067E-06	192.523008	11.9485627	1.23556005	0.17782581
0.006081053	0.000183343	3.45778E-05	4.7542E-06	187.653667	11.8629131	1.21799703	0.18062394
0.005877707	0.000176117	3.23511E-05	3.3979E-06	184.592838	8.55367851	1.19853648	0.13282283
0.00675364	0.000215493	5.84024E-05	6.8418E-06	212.003676	6.62066222	1.51014557	0.17663594
0.004731344	7.23378E-05	3.97496E-05	3.4229E-06	210.045741	9.93664721	1.48082653	0.14372069
0.005128685	0.000231847	4.01451E-05	4.1832E-06	204.180657	10.4092943	1.41932495	0.15163257
0.004716351	0.000206082	3.46839E-05	3.94E-06	198.827718	10.7547354	1.36934832	0.16156656
0.004711554	0.000230731	3.30133E-05	4.3074E-06	194.336107	12.0078746	1.33487608	0.18128574
0.00440867	0.000202006	3.00047E-05	3.0905E-06	191.290284	9.05396807	1.31722132	0.13656929
0.003941054	0.000139939	3.1886E-05	4.2397E-06	205.099596	7.42243021	1.42302254	0.18947254
0.003731041	0.00013119	2.93445E-05	3.2596E-06	202.402903	12.0089357	1.40174397	0.16950724
0.003726244	0.000146174	2.78957E-05	3.4341E-06	197.717684	12.7547651	1.36586638	0.18211356
0.003535704	0.000132006	2.59285E-05	2.2913E-06	195.72916	8.57682722	1.35155705	0.12339367
0.00380808	6.26027E-05	3.93615E-05	5.348E-06	220.510993	9.62848994	1.57014452	0.22258747
0.003008486	6.99132E-05	3.01216E-05	2.867E-06	218.528042	12.6602942	1.53471184	0.16724837
0.003005028	6.93284E-05	2.84259E-05	2.9446E-06	215.645821	13.3279601	1.46935978	0.17397091
0.002903342	7.09064E-05	2.58636E-05	2.9469E-06	208.257579	14.0748918	1.43282648	0.18655962
0.002870341	7.19191E-05	2.46438E-05	1.9985E-06	201.768606	9.38313851	1.42535737	0.12837008
0.002463486	6.07502E-05	2.53403E-05	3.4823E-06	220.788244	18.9164465	1.50677697	0.24116414
0.002510914	6.36266E-05	2.51748E-05	2.5515E-06	218.891808	18.9523834	1.48138724	0.19386792
0.002384394	6.35116E-05	2.27278E-05	2.5441E-06	213.197582	20.2389315	1.44597829	0.20870289
0.002377873	6.52187E-05	2.21092E-05	1.9236E-06	209.39979	21.4596373	1.4360555	0.18899217

0.0024511	7.7737E-05	2.60342E-05	4.6540E-06	222.028986	24.7844359	1.51711746	0.31695347
0.002304432	7.54346E-05	2.50163E-05	3.9025E-06	227.452363	23.990557	1.49214109	0.27670595
0.002341036	4.0066E-05	2.49662E-05	2.5291E-06	224.424578	21.1830736	1.4856464	0.20412467
0.002198327	7.86073E-05	2.24787E-05	2.4629E-06	219.275627	20.660228	1.45790667	0.20412398
0.002195479	8.04392E-05	2.19049E-05	1.9719E-06	217.15446	23.0432815	1.43642769	0.19283223

	E^* (kJ/mol)	v_0^* (cm^3/mol)	v_1^* (cm^3/mol*GPa)	D_0 (m^2/s) or η_o (Pa s)	R^2
O	75.636	1.315	-3.375E-03	2.089E-07	0.988
Mg	66.530	1.421	-5.046E-03	2.561E-07	0.988
Si	79.246	1.103	-2.584E-03	1.739E-07	0.980
viscosity	41.018	1.455	-4.777E-03	4.549E-04	0.998

Table 4. Parameters for self-diffusivities of O, Mg and Si are based on eq (5) in text; shear viscosity is based on eq (6). Numerical values for E* and V* in the table are given in rational units for ease of interpretation. Note that numerical values should be converted to SI units (m^3 for volume, J for energy and Pa for pressure) when computing values at specific p-T points. No unit conversions are required for the pre-exponential terms D_o and η_o.

ρ $\left(\frac{kg}{m^3}\right)$	$b(V)$ $\left(\frac{kJ}{K^{3/5}mol}\right)$	σ	$a(V)$ $\left(\frac{kJ}{mol}\right)$	σ
2753.83	4.518	0.011	-5803.4	1.5
3000.07	4.569	0.0043	-5825.9	0.58
3075.07	4.574		-5829.2	
3150.07	4.595	0.0067	-5833.4	0.91
3225.08	4.608		-5836.1	
3300.08	4.644	0.0099	-5839.7	1.3
3500.08	4.744	0.024	-5845.9	3.3
3800.09	5.122	0.016	-5871.2	2.3
3900.09	5.330	0.0084	-5886.8	1.3
4200.10	5.835	0.021	-5895.6	3.2
4350.10	6.094	0.015	-5890.3	2.3
4500.10	6.388	0.011	-5880.0	1.7

Table 5. Coefficients for the Rosenfeld-Tarazona (1998) model expression for the potential energy of a dense fluid: $U(V,T)=a(V)+b(V)T^{3/5}$. Model equations are compared to MD simulation data in Fig. 12.

i	$a(V)$ $\left(\frac{kJ}{mol}\right)$	$b(V)$ $\left(\frac{kJ}{K^{3/5}mol}\right)$
0	19790.2	52.7838
1	-437356.	-471.962
2	3046190.	1706.03
3	-11179100.	-2690.69
4	23103100.	1553.34
5	-26316700.	
6	14597600.4	
7	-2621980.	

Table 6. Polynomial parameterizations of the Rosenfeld-Tarazona (1998) functions for the potential energy: $a(V)=\sum_0^n a_i V^i$ and $b(V)=\sum_0^n b_i V^i$. V has units cm^3/gm or $1000\times$ the quantity in units of m^3/kg. See Fig. 13.

Parameter	Value	Units
V_v	8.08642×10^{-4}	m^3/kg
K_v	0.131575	*GPa*
$K_v^{'}$	11.8272	

Table 7. Parameterization of the Universal EOS (Eq. 9) along the nominal 3500 K isotherm (T_0 = 3582.75 ± 45.75 K). The standard error on residuals for pressure recovery from this EOS is 0.059 GPa.